Geophysical Journal International

Geophys. J. Int. (2012) **191,** 530–544 doi: 10.1111/j.1365-246X.2012.05625.x

A global model of electromagnetic coupling for nutations

Mathieu Dumberry[1] and Laurence Koot[1,2]

[1] *Department of Physics, University of Alberta, Edmonton,* T6G 2G7, *Canada. E-mail: dumberry@ualberta.ca*
[2] *Royal Observatory of Belgium, Brussels, Belgium*

Accepted 2012 July 24. Received 2012 July 24; in original form 2012 April 23

SUMMARY

Nutations are small variations in the orientation of the Earth's rotation axis in space. They are caused by the gravitational torque that the Moon, the Sun, and other planets exert on the equatorial bulge. As nutations involve differential rotations between the mantle, fluid core and inner core, the motion of each of these internal regions depends on the coupling between them. In particular, a coupling of a dissipative nature is required to match observations. One possibility is electromagnetic (EM) coupling at the inner and outer core boundaries, the focus of our study. Existing EM coupling models are based on a formulation where the perturbation variables and the equations they must satisfy are defined at local geographic points on the boundary. Here, we show how EM coupling models can be cast under a global formalism, where all variables are expanded in spherical harmonics. This formulation allows a separation of the contribution from the poloidal and toroidal parts of the EM torque, and we show that, under certain conductivity scenarios, this separation is important.

Key words: Earth rotation variations; Electromagnetic theory; Magnetic field; Core, outer core and inner core.

1 INTRODUCTION

Differential motion between two conducting regions stretches existing magnetic field lines that cross their boundary. The differential advection of magnetic field structures at the boundary also perturbs the original magnetic field. Both of these processes produce an induced secondary magnetic field and an associated tangential electromagnetic (EM) stress at the boundary. EM stress at the core–mantle boundary (CMB) produced in this fashion has been suggested long ago as a mechanism to transfer angular momentum between the mantle and the core, whether in the axial or equatorial direction (Rochester 1960, 1962, 1968).

The most detailed models of EM coupling to date are those that have been developed to study changes in the length of day (LOD) (Rochester 1960; Roberts 1972; Stix & Roberts 1984; Holme 1998). These models seek to determine the axial EM torque on the mantle produced by tangential core flows in the vicinity of the CMB. The calculation requires a known model of the magnetic field and its secular variation, the latter being inverted to recover core flows. All fields are expanded in terms of global basis functions, namely a truncated summation of surface spherical harmonics, and the formulation of the axial EM torque is expressed in terms of these global variables. The EM torque in the equatorial direction and associated changes in the polar motion can be computed with the same formalism (Greff-Lefftz & Legros 1995). An extension of these models makes it possible to include the effects of a non-uniform mantle conductivity structure (Holme 2000; Wicht & Jault 2000).

The influence of EM coupling at the CMB on the dynamics of Earth's rotation has also been considered in the modelling of precession (Toomre 1966; Rochester 1976), Earth's free wobbles (Rochester & Smylie 1965; Toomre 1974) and forced nutations (Sasao 1977; Gwinn *et al.* 1986; Buffett 1992). The models used in these studies are generally much simpler, in large part because the core motion can be considered as a simple rigid body rotation; to compute the EM torque, it is only sufficient to determine the misalignment of the rotation vectors of the core and mantle. Although the magnetic field geometry on which this differential rotation acts may be complex, the EM torque can be approximated by that produced by the combination of a simple axial dipole and a uniform radial field, the latter capturing the coupling effects from all non-dipolar parts (Buffett 1992).

In this work, we focus on EM coupling in the context of Earth's nutations. Because the mantle, fluid core and inner core have different ellipticities and different densities, each reacts differently to the imposed external tidal torque, leading to a differential rotation between them. Furthermore, forced nutations are amplified by the presence of free rotational modes of the Earth (which are characterized by differential rotation of its internal regions). Differential rotation at the CMB and inner core boundary (ICB) lead to internal torques, including EM torques, which in turn affect the nutation motion of each region.

Although the bulk of the nutation motion in the fluid core can be approximated by a rigid body rotation, coupling at the CMB and ICB introduces a secondary flow. In the context of EM coupling, the source of this flow is from the Lorentz force produced by

the interaction between the radial magnetic field and the secondary magnetic field induced by the differential motion at the boundaries. When the strength of the background radial magnetic field is larger than approximately 0.6 mT, this secondary flow is no longer negligible and must be taken into account in the computation of the EM torque (Buffett *et al.* 2002). While this feedback mechanism may not change significantly the EM torque at the CMB, where the radial magnetic field strength is estimated to be between 0.3 and 0.6 mT (e.g. Olsen *et al.* 2007), its effect is likely important when computing the torque at the ICB, where indirect inferences suggest that the field may be as large as a few mT (Christensen & Aubert 2006; Buffett 2010; Gillet *et al.* 2010).

This interaction between the secondary flow and magnetic field is incorporated in the EM coupling model for nutations developed by Buffett *et al.* (2002). This is done by developing the coupled equations governing the evolution of the secondary flow and the induced magnetic field at local coordinate points on the fluid-solid boundary. Only the perturbation in the two directions tangential to the boundary are solved for, as these dominate at leading order. Analytical solutions are found and depend on the local amplitude of the radial magnetic field. The EM torque is then evaluated by an integration over the spherical surface of these local solutions. Thus, in contrast to the models used in LOD studies, the EM coupling model developed for nutations is formulated in terms of variables defined at local coordinate points, rather than in terms of global basis functions.

Here, we show how the EM coupling model of Buffett *et al.* (2002) can be cast under a global formalism, with all variables expanded in surface spherical harmonics. Each of the flow perturbation and the induced magnetic field is separated into a poloidal and a toroidal contribution. Similarly, the EM torque is also separated into a poloidal and toroidal part. We develop our model both in the limit where the fluid core motion can be approximated by a rigid body rotation, and when the secondary flow from Lorentz forces must be considered.

Our approach is not entirely novel: in the theoretical development of his original model, Buffett (1992) also decomposed the induced magnetic field in its poloidal and toroidal contribution, each expanded in spherical harmonics. However, these two individual contributions to the EM torque were never actually computed; instead, the EM torque was determined on the basis of boundary conditions valid at local coordinate points. Another study in which the induced magnetic field is expanded in spherical harmonics is that of Greff-Lefftz & Legros (1999); however, their model only considered the case of a background magnetic field restricted to an axial dipole. In contrast, our formulation is valid for any background magnetic field morphology.

Our new formulation is based on the same approximations as used in the model of Buffett *et al.* (2002), and we show that we can recover their results. However, our global formulation reveals subtle aspects of the behaviour of the toroidal and poloidal parts of the EM torque. These effects are not apparent when adopting a local formulation (though they could be incorporated by an extension of the model).

2 FUNDAMENTALS

2.1 Nutation motion

Nutations involve small periodic perturbations in the rotation vector with respect to Earth's mean rotation defined as $\mathbf{\Omega}_o = \Omega_o \hat{\mathbf{z}}$. To first order, the velocity field within each of the mantle, fluid outer core (FOC) and solid inner core (SIC) associated with Earth's nutations is that of a rigid-body rotation. Their rotation vectors are defined, respectively, by

$$\mathbf{\Omega}(t) = \Omega_o \hat{\mathbf{z}} + \boldsymbol{\omega}(t)\,, \tag{1a}$$

$$\mathbf{\Omega}_f(t) = \Omega_o \hat{\mathbf{z}} + \boldsymbol{\omega}(t) + \boldsymbol{\omega}_f(t)\,, \tag{1b}$$

$$\mathbf{\Omega}_s(t) = \Omega_o \hat{\mathbf{z}} + \boldsymbol{\omega}(t) + \boldsymbol{\omega}_s(t)\ . \tag{1c}$$

The vector $\boldsymbol{\omega}(t)$ characterizes the perturbation in rotation of the mantle; its equatorial components characterize nutations whereas its axial component captures variations in the rotation rate. To first order, equatorial and axial rotation perturbations are decoupled (e.g. Munk & MacDonald 1960) so that the nutational part of the motion can be represented by:

$$\boldsymbol{\omega}(t) = \omega_x(t)\,\hat{\mathbf{x}} + \omega_y(t)\,\hat{\mathbf{y}}\,, \tag{2}$$

where $\hat{\mathbf{x}}$ points towards longitude $= 0$. The vectors $\boldsymbol{\omega}_f(t)$ and $\boldsymbol{\omega}_s(t)$ characterize the rotational variation of the FOC and SIC, respectively, with respect to the mantle and are defined in a similar manner. The amplitude of these perturbations are of the order of 10^6 times smaller than Ω_o.

By projecting the $\hat{\mathbf{x}} - \hat{\mathbf{y}}$ plane onto a complex plane, we can use a compact notation where we define

$$\tilde{\omega}(t) = \omega_x(t) + \mathrm{i}\,\omega_y(t)\,, \tag{3}$$

and use similar definitions for $\tilde{\omega}_f(t)$ and $\tilde{\omega}_s(t)$. Temporal variations in $\tilde{\omega}(t)$, $\tilde{\omega}_f(t)$ and $\tilde{\omega}_s(t)$ are described by a rotation about $\hat{\mathbf{z}}$ at a frequency ω, namely

$$\tilde{\omega}(t) = \hat{\omega}\, e^{\mathrm{i}\omega t}\,, \quad \tilde{\omega}_f(t) = \hat{\omega}_f\, e^{\mathrm{i}\omega t}\,, \quad \tilde{\omega}_s(t) = \hat{\omega}_s\, e^{\mathrm{i}\omega t}\,. \tag{4}$$

The complete nutation motion is obtained by a summation of motion each with its own tidal frequency ω. In a frame attached to the rotating Earth, each of these tidal frequencies are small perturbations from $\omega = -\Omega_o$, the minus sign indicating that the motion is retrograde.

Torques between the mantle, FOC and SIC arise when these regions are differentially rotating with respect to one another. Here, we focus on the EM torque that results from the differential nutation motion at both the CMB and ICB. In the formulation that we use, it is convenient to expand all velocities with respect to a frame fixed to the rigid nutation motion of the FOC (i.e. a frame rotating at angular velocity $\mathbf{\Omega}_f$). The nutation velocity field $\mathbf{v}_n$ when viewed in this frame is

$$\mathbf{v}_n = \boldsymbol{\Delta\omega}(t) \times \mathbf{r}\,. \tag{5a}$$

where

$$\begin{aligned} \boldsymbol{\Delta\omega}(t) &= -\boldsymbol{\omega}_f(t) && \text{in the mantle} \\ &= \mathbf{0} && \text{in the FOC} \\ &= \boldsymbol{\omega}_s(t) - \boldsymbol{\omega}_f(t) && \text{in the SIC.} \end{aligned} \tag{5b}$$

We adopt a general formulation and define

$$\Delta\tilde{\omega}_b(t) = \Delta\hat{\omega}_b\, e^{\mathrm{i}\omega t} \tag{6}$$

to represent the nutation of the solid region at a boundary at $r = r_b$ with respect to the FOC. When differential rotation at the CMB ($r_b = r_f$) is considered, $\Delta\hat{\omega}_b = -\hat{\omega}_f$, whereas at the ICB ($r_b = r_s$), $\Delta\hat{\omega}_b = \hat{\omega}_s - \hat{\omega}_f$. Futhermore, we decompose $\mathbf{v}_n$ according to

$$\mathbf{v}_n = \boldsymbol{\nabla} \times (\mathcal{T}_n\, \mathbf{r}), \tag{7}$$

where the toroidal scalar $\mathcal{T}_n$ is given by

$$\mathcal{T}_n = -\mathrm{Re}\left[r\,\Delta\hat{\omega}_b\, e^{\mathrm{i}\omega t}\, Y_1^1 \right], \tag{8}$$

and where

$$Y_1^1 = P_1^1(\cos\theta)\, e^{-\mathrm{i}\phi} = -\sin\theta\, e^{-\mathrm{i}\phi} \tag{9}$$

is the surface spherical harmonic of degree $l = 1$ and order $m = 1$ defined with the following convention,

$$Y_l^m = Y_l^m(\theta,\phi) = P_l^m(\cos\theta)\, e^{-\mathrm{i}m\phi}, \tag{10}$$

where the functions P_l^m are associated Legendre Polynomials, with θ and ϕ being the co-latitude and longitude, respectively. The P_l^m are normalized such that

$$\int_\Omega (Y_l^m)^* Y_{l'}^{m'}\, d\Omega = N_{lm}\,\delta_{ll'}\delta_{mm'}, \tag{11}$$

where the integration is taken over a unit sphere and where

$$N_{lm} = \frac{4\pi}{2l+1}\frac{(l+m)!}{(l-m)!}. \tag{12}$$

2.2 Mathematical representation of the magnetic field

A magnetic field $\mathbf{B_o}$ that permeates the whole Earth is maintained by convective motion in the Earth's fluid core. Evolution of the large length scale component of this magnetic field occurs over a timescale of decades to hundreds of years (Jackson *et al.* 2000). Since nutations involve diurnal timescale motion, $\mathbf{B_o}$ can be considered as a steady, background magnetic field. In spherical geometry, $\mathbf{B_o}$ within the Earth can be conveniently written in terms of a poloidal–toroidal representation (e.g. Gubbins & Roberts 1987),

$$\mathbf{B_o} = \nabla\times\nabla\times(\mathcal{S}_o\,\mathbf{r}) + \nabla\times(\mathcal{T}_o\,\mathbf{r}), \tag{13}$$

where $\mathbf{r}$ is the radial position vector and $\mathcal{S}_o$ and $\mathcal{T}_o$ are scalars containing respectively the information on the poloidal and toroidal part of the field. According to this definition, the horizontal components of $\mathbf{B_o}$ at a radius r are given by

$$B_\theta = \frac{1}{\sin\theta}\frac{\partial\mathcal{T}_o}{\partial\phi} + \frac{1}{r}\frac{\partial}{\partial\theta}\left(\frac{\partial}{\partial r} r\mathcal{S}_o\right), \tag{14a}$$

$$B_\phi = -\frac{\partial\mathcal{T}_o}{\partial\theta} + \frac{1}{r\,\sin\theta}\frac{\partial}{\partial\phi}\left(\frac{\partial}{\partial r} r\mathcal{S}_o\right). \tag{14b}$$

The radial part of the field $\mathbf{B}_\mathrm{o}$ is contained entirely in the poloidal scalar $\mathcal{S}_o$, and is given by

$$B_r = \frac{\mathcal{L}^2\mathcal{S}_o}{r}, \tag{14c}$$

where $\mathcal{L}$ is the angular momentum operator of quantum mechanics (e.g. Edmonds 1960). Since a toroidal magnetic field does not have a radial component, toroidal field lines must form closed loops on spherical surfaces.

2.3 Magnetic field and flow perturbations

Differential rotation at fluid-solid boundaries stretches and advects the background magnetic field $\mathbf{B_o}$. This causes a small perturbation in the magnetic field, a secondary field which we denote by $\mathbf{b}$ and expand in terms of a poloidal–toroidal decomposition

$$\mathbf{b} = \nabla\times\nabla\times(\mathcal{S}_b\,\mathbf{r}) + \nabla\times(\mathcal{T}_b\,\mathbf{r}), \tag{15a}$$

with

$$\mathcal{T}_b = \sum_{l,m}\mathrm{Re}\left[t_{lm}^b\, Y_l^m\, e^{\mathrm{i}\omega t}\right], \tag{15b}$$

$$\mathcal{S}_b = \sum_{l,m}\mathrm{Re}\left[s_{lm}^b\, Y_l^m\, e^{\mathrm{i}\omega t}\right], \tag{15c}$$

and where

$$\sum_{l,m} \equiv \sum_{l=1}^{\infty}\sum_{m=-l}^{l}. \tag{16}$$

Vectorial components of $\mathbf{b}$ in spherical coordinates, b_r, b_θ and b_ϕ, are defined by expressions similar to those in eq. (14). We have explicitly assumed a time-dependency of the form $e^{\mathrm{i}\omega t}$ because the nutation motion is the only source of $\mathbf{b}$ in our system. Under the representation of (15), the coefficients t_{lm}^b and s_{lm}^b depend only on radial position.

Coupling with both the mantle and SIC induce small perturbations in the velocity field of the FOC, $\mathbf{v}$, with respect to the rigid body nutation motion. The origin of these perturbations includes viscous and pressure forces associated with the differentially rotating ellipsoidal boundaries, as well as those induced by Lorentz force produced by the interaction between $\mathbf{B_o}$ and $\mathbf{b}$. Here, we concentrate on the latter. Assuming the perturbed flow is incompressible, $\nabla\cdot\mathbf{v} = 0$, we expand $\mathbf{v}$ as

$$\mathbf{v} = \nabla\times\nabla\times(\mathcal{S}_f\,\mathbf{r}) + \nabla\times(\mathcal{T}_f\,\mathbf{r}), \tag{17a}$$

where the toroidal ($\mathcal{T}_f$) and poloidal ($\mathcal{S}_f$) scalar functions at a given radius are further expanded in terms of surface spherical harmonics

$$\mathcal{T}_f = \sum_{l,m}\mathrm{Re}\left[t_{lm}^f\, Y_l^m\, e^{\mathrm{i}\omega t}\right], \tag{17b}$$

$$\mathcal{S}_f = \sum_{l,m}\mathrm{Re}\left[s_{lm}^f\, Y_l^m\, e^{\mathrm{i}\omega t}\right]. \tag{17c}$$

2.4 Approximations

The induction equation that governs the changes in $\mathbf{b}$, in a frame fixed to the rigid nutation motion of the FOC, is given by

$$\frac{\partial\mathbf{b}}{\partial t} + \nabla\times(\eta\nabla\times\mathbf{b}) = \nabla\times(\mathbf{v}_t\times\mathbf{B}), \tag{18}$$

where $\mathbf{B} = \mathbf{B_o} + \mathbf{b}$ and where η is the magnetic diffusivity, defined as $\eta = 1/\sigma\mu$, where σ the electrical conductivity and μ the permeability of free space. Here, the velocity $\mathbf{v}_t$ contains both the flow perturbation $\mathbf{v}$ and the rigid-body nutation motion $\mathbf{v}_n$,

$$\mathbf{v}_t = \mathbf{v}_n + \mathbf{v}. \tag{19}$$

The contribution from the background velocity field responsible for the (slow) secular variation of the magnetic field is not included in $\mathbf{v}_t$ because its effect on the diurnal changes in $\mathbf{b}$ associated with nutations is negligible (Buffett 1992). Specifying the velocity in this manner is convenient because eq. (18) is then valid in any region of space; its right-hand side represents the electromotive force (e.m.f.) from the total velocity viewed in the frame rotating with the FOC. Evidently, in both the mantle and SIC $\mathbf{v}_t = \mathbf{v}_n$, whereas $\mathbf{v}_t = \mathbf{v}$ in the FOC.

We anticipate $\mathbf{b}$ to be much weaker than $\mathbf{B_o}$ and we use the linearized form of the induction equation

$$\frac{\partial\mathbf{b}}{\partial t} - \eta\nabla^2\mathbf{b} = -\mathbf{v}_t\cdot\nabla\mathbf{B_o} + \mathbf{B_o}\cdot\nabla\mathbf{v}_t, \tag{20}$$

where we have assumed a constant conductivity and where the operator ∇^2 is defined as

$$\nabla^2 = \frac{1}{r}\frac{\partial^2}{\partial r^2} r \; - \frac{\mathcal{L}^2}{r^2} \,. \tag{21}$$

The relative contribution from the two terms in (21) can be obtained by considering the characteristic length scale of propagation for a periodic perturbation, which is given by the magnetic skin-depth (e.g. Gubbins & Roberts 1987)

$$\delta = \sqrt{\frac{2\eta}{|\omega|}} \,. \tag{22}$$

The electrical conductivity of the fluid and solid cores are not known very precisely, though a typical estimate is $\sigma = 5 \times 10^5$ S m^{-1} (Stacey & Anderson 2001). The frequencies of the forced nutations are all close to diurnal, so $|\omega| = \Omega_o = 7.29 \times 10^{-5}$ s^{-1} and this implies that $\eta \approx 1.6$ m^2 s^{-1} and $\delta \approx 200$ m. This suggests

$$\frac{\delta}{r} \sim 10^{-4} \,, \tag{23}$$

and thus, for a given magnetic field perturbations of spherical harmonic degree l, we expect that

$$\frac{\partial}{\partial r} \approx \frac{1}{\delta} \,, \tag{24}$$

whereas horizontal variations are of the order of l/r. This means that as long as we consider the large length scale part of the magnetic field (i.e. $l \ll 10^4$), horizontal derivatives are much smaller than radial derivatives, and

$$\frac{\partial}{\partial r} \gg \frac{1}{r}\frac{\partial}{\partial \theta} \,, \frac{1}{r}\frac{\partial}{\partial \phi} \,. \tag{25a}$$

Further,

$$\frac{\partial^2}{\partial r^2} \gg \frac{1}{r}\frac{\partial}{\partial r} \gg \frac{1}{r^2} \,, \qquad \nabla^2 \approx \frac{\partial^2}{\partial r^2} \,. \tag{25b}$$

The approximations in eq. (25) are employed throughout our study. Even when coupling at the CMB is considered, where the conductivity of the lower mantle may be weaker by four orders of magnitude (e.g. Constable 2007), $\delta/r \sim 10^{-2}$, and these approximations are valid as long as $l \ll 100$.

Given that nutations only sample a region of ∼200 m above and below the ICB, the approximation of constant conductivity is justified at that boundary. A constant conductivity in the lower mantle is more difficult to justify. Here, in the absence of a well-known model, we take the simplest approach and assume a constant conductivity at the base of the mantle, though we need to remain alert to the fact that it represents an 'effective' conductivity.

According to eq. (23), the solenoidal condition $\boldsymbol{\nabla} \cdot \mathbf{b} = 0$ implies that we expect $b_r \ll b_\theta \,, b_\phi$; in fact,

$$\frac{|b_r|}{|\hat{\mathbf{r}} \times \mathbf{b}|} \approx \frac{\delta}{r} \,. \tag{26}$$

We expect that a similar scaling applies for flow perturbation in the FOC and thus, to first order,

$$\mathbf{v} \cdot \boldsymbol{\nabla} \mathbf{B_o} \approx r^{-1} \, \mathbf{v}_H \cdot \boldsymbol{\nabla}_1 \mathbf{B_o} \tag{27a}$$

$$\mathbf{B_o} \cdot \boldsymbol{\nabla} \mathbf{v} \approx B_r \frac{\partial}{\partial r} \mathbf{v}, \tag{27b}$$

where $\mathbf{v}_H$ is the horizontal part of the flow and where

$$\boldsymbol{\nabla}_1 = r \boldsymbol{\nabla} - \mathbf{r} \frac{\partial}{\partial r} \tag{28}$$

is the dimensionless surface gradient on a unit sphere.

2.5 Induction equation

With the approximations of the preceding section, the induction equation, in the frame of the FOC, valid in all region of space, can thus be written as

$$\frac{\partial \mathbf{b}}{\partial t} \; - \eta \nabla^2 \mathbf{b} \; = -r^{-1} \, (\mathbf{v}_n + \mathbf{v}_H) \cdot \boldsymbol{\nabla}_1 \mathbf{B_o} + B_r \frac{\partial}{\partial r} (\mathbf{v}_n + \mathbf{v}) \,. \tag{29}$$

The rigid-body nutation motion $\mathbf{v}_n$ is purely toroidal, whereas the horizontal part of the perturbation flow includes both a toroidal and a poloidal part,

$$\mathbf{v}_H = \boldsymbol{\nabla}_1 \times \mathcal{T}_f \hat{\mathbf{r}} \; + \boldsymbol{\nabla}_1 \left(\frac{1}{r} \frac{\partial}{\partial r} r \mathcal{S}_f \right) \,. \tag{30}$$

The radial derivative of $\mathbf{v}_n$ is non-zero only at a fluid-solid boundaries located at $r = r_b$, where we can write

$$\frac{\partial \mathbf{v}_n}{\partial r} \propto \delta(r - r_b) \,, \tag{31}$$

where $\delta(r)$ is the delta function. Thus, this term in eq. (29) represents a source of $\mathbf{b}$ at $r = r_b$ induced by the differential nutation motion, if the region of space considered straddles the ICB or CMB. If we restrict eq. (29) to only include one region of space (mantle, FOC or SIC), this source term can be dropped from the equation (it re-enters through continuity conditions at $r = r_b$). Eq. (29) is decomposed into an equation for $\mathcal{T}_b$, by taking $\mathbf{r} \cdot \boldsymbol{\nabla} \times$ of eq. (29) and using (15) and (17),

$$\left[\frac{\partial}{\partial t} \; - \eta \frac{\partial^2}{\partial r^2} \right] \mathcal{L}^2 \mathcal{T}_b \; = \\ - \boldsymbol{\nabla}_1 \cdot \left[B_r \boldsymbol{\nabla}_1 \frac{\partial \mathcal{T}_f}{\partial r} \right] + \left[\boldsymbol{\nabla}_1 \times \frac{\partial^2 \mathcal{S}_f}{\partial r^2} \hat{\mathbf{r}} \right] \cdot \boldsymbol{\nabla}_1 B_r \,, \tag{32a}$$

and an equation for $\mathcal{S}_b$, by taking $\mathbf{r} \cdot \boldsymbol{\nabla} \times \boldsymbol{\nabla} \times$ of eq. (29) and integrating once in the radial direction from infinity to r,

$$\left[\frac{\partial}{\partial t} \; - \eta \frac{\partial^2}{\partial r^2} \right] \mathcal{L}^2 \frac{\partial \mathcal{S}_b}{\partial r} \; = \\ -\boldsymbol{\nabla}_1 \cdot \left[B_r \boldsymbol{\nabla}_1 \frac{\partial^2 \mathcal{S}_f}{\partial r^2} \right] - \left[\boldsymbol{\nabla}_1 \times \frac{\partial \mathcal{T}_f}{\partial r} \hat{\mathbf{r}} \right] \cdot \boldsymbol{\nabla}_1 B_r \,. \tag{32b}$$

Note that the approximations of eq. (25) have been used in both these derivations. We thus have two equations, one each for the poloidal and toroidal perturbation of the magnetic field. We recall that these equations are valid in either the FOC, mantle and SIC. In the solid regions, since $\mathcal{T}_f = \mathcal{S}_f = 0$ due to the absence of flow, these equations simplify to

$$\left[\frac{\partial}{\partial t} \; - \eta_s \frac{\partial^2}{\partial r^2} \right] \mathcal{L}^2 \mathcal{T}_b^s \; = 0 \,, \tag{33a}$$

$$\left[\frac{\partial}{\partial t} \; - \eta_s \frac{\partial^2}{\partial r^2} \right] \mathcal{L}^2 \frac{\partial \mathcal{S}_b^s}{\partial r} \; = 0 \,. \tag{33b}$$

Note that using the approximations of eq. (25) the horizontal components of (29) are

$$\left(\frac{\partial}{\partial t} \; - \eta \frac{\partial^2}{\partial r^2} \right) b_{\theta,\phi} = B_r \frac{\partial}{\partial r} v_{\theta,\phi} \,. \tag{34}$$

These represent conditions that are valid at any θ, ϕ coordinate points on a spherical surface and are identical to eqs (7)–(8) of Buffett *et al.* (2002). Furthermore, we can recover eq. (32) by applying $\mathbf{r} \cdot \boldsymbol{\nabla} \times$ and $\mathbf{r} \cdot \boldsymbol{\nabla} \times \boldsymbol{\nabla} \times$ on the vectorial form of eq. (34). In other words, though expressed in a different form, eqs (32a and b) are identical to the induction equation used in Buffett *et al.* (2002).

However, we note that keeping the first term on the right-hand side of eq. (29) is necessary to describe fully the induction equation in the radial direction. Indeed, an equivalent expression to (32b) is obtained by taking the radial derivative of the radial part of eq. (29) (and neglecting curvature terms).

2.6 Momentum equation

The interaction between the background magnetic field $\mathbf{B_o}$ and the secondary magnetic field $\mathbf{b}$ leads to a Lorentz force on the fluid. This creates a flow perturbation $\mathbf{v}$ in the otherwise rigidly rotating FOC. In the reference frame rotating with the FOC, the momentum equation that governs the evolution of $\mathbf{v}$, in the inviscid limit, in the absence of buoyancy forces and linearized for small $\mathbf{v}$ and $\mathbf{b}$, is given by

$$\frac{\partial \mathbf{v}}{\partial t} + 2\boldsymbol{\Omega}_f \times \mathbf{v} + \frac{\partial \boldsymbol{\Omega}_f}{\partial t} \times \mathbf{r} + \boldsymbol{\Omega}_f \times \boldsymbol{\Omega}_f \times \mathbf{r} = -\boldsymbol{\nabla}\left(\frac{p}{\rho}\right) + \frac{1}{\rho\mu}\left(\mathbf{B_o}\cdot\boldsymbol{\nabla}\mathbf{b} + \mathbf{b}\cdot\boldsymbol{\nabla}\mathbf{B_o}\right), \tag{35}$$

where ρ is density and p includes both the dynamic and magnetic pressure. Since $\mathbf{v} = \mathbf{0}$ in the absence of Lorentz forces, we can identify a pressure component (p_Ω) associated with the rigid rotation of the FOC,

$$\frac{\partial \boldsymbol{\Omega}_f}{\partial t} \times \mathbf{r} + \boldsymbol{\Omega}_f \times \boldsymbol{\Omega}_f \times \mathbf{r} = -\boldsymbol{\nabla}\left(\frac{p_\Omega}{\rho}\right). \tag{36}$$

This part remains unaltered if $\boldsymbol{\Omega}_f$ is unchanged by the Lorentz force. This is the case if the flow perturbation from EM coupling is restricted to boundary layers; then, sufficiently far away from the boundary, $\mathbf{v}$ should vanish and the only non-zero part of eq. (35) is given by eq. (36). This is never strictly true because inertial and Magnetic-Coriolis (MC) waves initiated in the boundary layer can propagate through the whole FOC. If we assume that $\mathbf{v} = \mathbf{0}$ far away from the boundary, this amounts to neglecting the effects of these waves in the nutation dynamics, as was done in the model of Buffett *et al.* (2002). We follow the same approach here, in which case the part of the pressure associated with eq. (36) can be removed from eq. (35). Further, $\boldsymbol{\Omega}_f$ differs only slightly from $\Omega_o\hat{\mathbf{z}}$ (by approximately 10^{-6} in magnitude); for mathematical convenience, we can replace the former by the latter in the Coriolis term, and the changes in $\mathbf{v}$ are expressed by

$$\frac{\partial \mathbf{v}}{\partial t} + 2\Omega_o(\hat{\mathbf{z}}\times\mathbf{v}) = -\boldsymbol{\nabla}\left(\frac{p'}{\rho}\right) + \frac{1}{\rho\mu}\left(\mathbf{B_o}\cdot\boldsymbol{\nabla}\mathbf{b} + \mathbf{b}\cdot\boldsymbol{\nabla}\mathbf{B_o}\right), \tag{37}$$

where p' is the perturbation in pressure associated with $\mathbf{v}$ and $\mathbf{b}$.

As was the case for the induction equation, the dominance of radial derivatives over lateral derivatives, and the fact that $b_r \ll b_\theta$, b_ϕ allows us to write

$$\mathbf{B_o}\cdot\boldsymbol{\nabla}\mathbf{b} + \mathbf{b}\cdot\boldsymbol{\nabla}\mathbf{B_o} \approx r^{-1}\mathbf{b}_H\cdot\boldsymbol{\nabla}_1\mathbf{B_o} + B_r\frac{\partial \mathbf{b}}{\partial r}. \tag{38}$$

Taking $\mathbf{r}\cdot\boldsymbol{\nabla}\times$ and $\mathbf{r}\cdot\boldsymbol{\nabla}\times\boldsymbol{\nabla}\times$ of eq. (37), we obtain, respectively,

$$\left[\frac{\partial}{\partial t} - 2\Omega_o\frac{\partial}{\partial\phi}\right]\mathcal{L}^2\mathcal{T}_f - 2\Omega_o\left[\cos\theta\mathcal{L}^2 + \sin\theta\frac{\partial}{\partial\theta}\right]\frac{\partial \mathcal{S}_f}{\partial r} = -\frac{1}{\rho\mu}\boldsymbol{\nabla}_1\cdot\left[B_r\boldsymbol{\nabla}_1\frac{\partial \mathcal{T}_b}{\partial r}\right] + \frac{1}{\rho\mu}\left[\boldsymbol{\nabla}_1\times\frac{\partial^2\mathcal{S}_b}{\partial r^2}\hat{\mathbf{r}}\right]\cdot\boldsymbol{\nabla}_1 B_r, \tag{39a}$$

$$\left[\frac{\partial}{\partial t} - 2\Omega_o\frac{\partial}{\partial\phi}\right]\mathcal{L}^2\frac{\partial^2\mathcal{S}_f}{\partial r^2} + 2\Omega_o\left[\cos\theta\mathcal{L}^2 + \sin\theta\frac{\partial}{\partial\theta}\right]\frac{\partial \mathcal{T}_f}{\partial r} = -\frac{1}{\rho\mu}\boldsymbol{\nabla}_1\cdot\left[B_r\boldsymbol{\nabla}_1\frac{\partial^3\mathcal{S}_b}{\partial r^3}\right] - \frac{1}{\rho\mu}\left[\boldsymbol{\nabla}_1\times\frac{\partial^2\mathcal{T}_b}{\partial r^2}\hat{\mathbf{r}}\right]\cdot\boldsymbol{\nabla}_1 B_r. \tag{39b}$$

Note that using the approximations of eq. (25) the horizontal components of eq. (37) are

$$\frac{\partial}{\partial t}v_{\theta,\phi} + f_{\theta,\phi}v_{\phi,\theta} = -\frac{B_r}{\rho\mu}\frac{\partial}{\partial r}b_{\theta,\phi}, \tag{40}$$

where $f_\theta = -2\Omega_o\cos\theta$ and $f_\phi = 2\Omega_o\cos\theta$ and where we have omitted the pressure term. The vectorial form of eq. (40) is akin to a momentum equation valid at any point on a spherical surface. Taking its radial derivative, one obtains the equations for v_θ and v_ϕ used in Buffett *et al.* (2002). We can recover eqs (39a and b) by applying $\mathbf{r}\cdot\boldsymbol{\nabla}\times$ and $\mathbf{r}\cdot\boldsymbol{\nabla}\times\boldsymbol{\nabla}\times$ on the vectorial form of eq. (40) and it follows that expressing the perturbation in the flow as in eq. (39) is identical to the formulation used in Buffett *et al.* (2002).

2.7 Boundary conditions

Since flow cannot penetrate a rigid boundary, the radial component of the flow at $r = r_b$ must equal zero. This imposes the condition

$$\mathcal{S}_f = 0. \tag{41}$$

In the inviscid limit, the flow cannot exert a lateral stress on the boundary. This stress-free condition requires that the radial derivative of the flow tangential to the boundary must vanish at $r = r_b$, which implies

$$\frac{\partial \mathcal{T}_f}{\partial r} = \frac{\partial^2\mathcal{S}_f}{\partial r^2} = 0. \tag{42}$$

The magnetic field perturbations on the fluid and solid side of the boundary are connected through continuity conditions. The continuity of the radial part of the magnetic field,

$$[\hat{\mathbf{r}}\cdot\mathbf{b}]^+_- = 0, \tag{43}$$

where $[X]^+_-$ denotes a jump in quantity X across the boundary, leads to the condition

$$\mathcal{S}_b = \mathcal{S}_b^s, \tag{44}$$

where the superscript s denotes a quantity in the solid region. Continuity of the tangential part of the magnetic field,

$$[\hat{\mathbf{r}}\times\mathbf{b}]^+_- = \mathbf{0}, \tag{45}$$

leads to the conditions

$$\mathcal{T}_b = \mathcal{T}_b^s, \tag{46}$$

$$\frac{\partial \mathcal{S}_b}{\partial r} = \frac{\partial \mathcal{S}_b^s}{\partial r}, \tag{47}$$

where we have used (44).

The induction equations involves second-order derivatives on $\mathcal{T}_b$ and third-order derivatives on $\mathcal{S}_b$; two more conditions are required at $r = r_b$. These are obtained from the continuity of the tangential electric field expressed by

$$[\eta\,\hat{\mathbf{r}}\times(\boldsymbol{\nabla}\times\mathbf{b})]^+_- = [\hat{\mathbf{r}}\times(\mathbf{v}_t\times\mathbf{B_o})]^+_-. \tag{48}$$

Using $\mathbf{v}_t = \mathbf{v}_n$ on the solid side and $\mathbf{v}_t = \mathbf{v}$ on the liquid side, we get:

$$\eta_s\,\hat{\mathbf{r}}\times(\boldsymbol{\nabla}\times\mathbf{b}_s) - \eta\,\hat{\mathbf{r}}\times(\boldsymbol{\nabla}\times\mathbf{b}) = \hat{\mathbf{r}}\times[(\mathbf{v}_n - \mathbf{v})\times\mathbf{B_o}]. \tag{49}$$

Note that this boundary condition is valid at both the CMB and the ICB. To get conditions on $\mathcal{T}_b$ and $\mathcal{S}_b$ we apply $\nabla \cdot [\hat{\mathbf{r}}\times \ldots]$ and $\nabla\cdot$ to eq. (49), which gives, respectively

$$\eta\frac{\partial}{\partial r}\mathcal{L}^2\mathcal{T}_b - \eta_s\frac{\partial}{\partial r}\mathcal{L}^2\mathcal{T}_b^s = \nabla_1\cdot\left[B_r\nabla_1(\mathcal{T}_f-\mathcal{T}_n)\right] - \left[\nabla_1\times\frac{\partial\mathcal{S}_f}{\partial r}\hat{\mathbf{r}}\right]\cdot\nabla_1 B_r\,, \tag{50}$$

$$\eta\frac{\partial^2}{\partial r^2}\mathcal{L}^2\mathcal{S}_b - \eta_s\frac{\partial^2}{\partial r^2}\mathcal{L}^2\mathcal{S}_b^s = \left[\nabla_1\times(\mathcal{T}_f-\mathcal{T}_n)\hat{\mathbf{r}}\right]\cdot\nabla_1 B_r - B_r\frac{\partial}{\partial r}\mathcal{L}^2\mathcal{S}_f\,, \tag{51}$$

where $\mathcal{T}_f$ and $\mathcal{S}_f$ on the right-hand sides are evaluated at the boundary. These conditions imply that the radial derivative of the tangential magnetic field is discontinuous across the boundary. This expresses the fact that eq. (29) involves a singular source at the boundary.

To close the system, additional boundary conditions on $\mathcal{T}_b$ and $\partial\mathcal{S}_b/\partial r$ must be specified at $r = r_b + \infty$ and $r = r_b - \infty$. We impose that perturbations are confined to the boundary layers (see Section 2.6), implying that $\mathcal{T}_b$ and $\partial\mathcal{S}_b/\partial r$ must equal zero far away from the boundary.

2.8 Sources of $\mathcal{S}_b$ and $\mathcal{T}_b$

Differential nutation motion at boundaries, captured by the presence of $\mathcal{T}_n$ on the right-hand side of eqs. (50–51), acts as a source of both toroidal and poloidal magnetic field. The origin of the poloidal perturbation is from the differential advection of the background poloidal field ($\mathcal{S}_o$) on either side of the boundary. This leads to a discontinuity in $\mathcal{S}_o$, which is accommodated by a secondary field $\mathcal{S}_b$ such that the magnetic field remains continuous across the boundary (Fig. 1a). The secondary field thus created subsequently evolves according to the eqs. (32b) and (33b) on the fluid and solid side of the boundary, respectively. Obviously, if $\mathcal{S}_o$ has no horizontal gradients, for instance as in the case of a uniform radial field, no discontinuity is introduced by the differential motion and no secondary field is generated.

The toroidal perturbation $\mathcal{T}_b$ results from the stretching of the poloidal field $\mathcal{S}_o$ by the differential motion at the boundary (Fig. 1b). This occurs whether the field has tangential gradients or not; thus in contrast to $\mathcal{S}_b$, a toroidal perturbation $\mathcal{T}_b$ is induced even in the case of a uniform radial background field.

On the basis of the source terms in eqs (50)–(51), an order of magnitude estimate for both $\mathcal{T}_b$ and $\partial\mathcal{S}_b/\partial r$ can be obtained. Using (22), and assuming equal conductivities on both sides of the boundary,

$$|\mathcal{T}_b| \approx \left|\frac{\partial\mathcal{S}_b}{\partial r}\right| \approx B_r\frac{r_b}{\delta}\frac{\Delta\hat{\omega}_b}{\Omega_o}\,. \tag{52}$$

Although $r_b/\delta \sim 10^4$, $\Delta\hat{\omega}_b/\Omega_o$ is of the order of 10^{-6} or smaller, so $|\hat{\mathbf{r}}\times\mathbf{b}| \ll B_r$.

If the conductivity on one side of the boundary is zero, then no radial electrical currents can penetrate this region and therefore no toroidal field is induced: $\mathcal{T}_b = 0$. Similarly, the background poloidal field can diffuse instantly in insulating regions, so no $\mathcal{S}_b$ is required to maintain continuity of the poloidal field. Thus, there would be no perturbation in the magnetic field at the boundary and no EM torque between the two regions. This would be the case at the CMB if the mantle is an insulator.

We note that differential motion at the boundary also advects structures of the background toroidal field $\mathcal{T}_o$, which acts as an additional source of $\mathcal{T}_b$. However, the amplitude of $\mathcal{T}_b$ from this effect is smaller than that from stretching of B_r by a factor δ/r_b and can be neglected provided the background toroidal field is of the same order or smaller than the background radial field. Since toroidal fields do not have radial components, there is no stretching of $\mathcal{T}_o$ by the differential motion.

2.9 Electromagnetic torque

The EM torque between two spherical shells, separated at radius r_b, can be written in terms of the surface integral of the EM stress at their boundary (Rochester 1960),

$$\mathbf{\Gamma} = \frac{r_b^3}{\mu}\int_\Omega (\hat{\mathbf{r}}\times\mathbf{B})(\mathbf{B}\cdot\hat{\mathbf{r}})\,d\Omega\,, \tag{53}$$

where $\mathbf{B} = \mathbf{B_o} + \mathbf{b}$, and the integral is taken over a unit sphere. The above expression represents a general formulation of the EM torque; the torque that the mantle exerts on the FOC is obtained by setting $r_b = r_f$, while the torque that the FOC exerts on the SIC is obtained by setting $r_b = r_i$. To first order,

$$(\hat{\mathbf{r}}\times\mathbf{B})(\mathbf{B}\cdot\hat{\mathbf{r}}) \approx (\hat{\mathbf{r}}\times\mathbf{b})\,B_r + (\hat{\mathbf{r}}\times\mathbf{B_o})\,b_r\,, \tag{54}$$

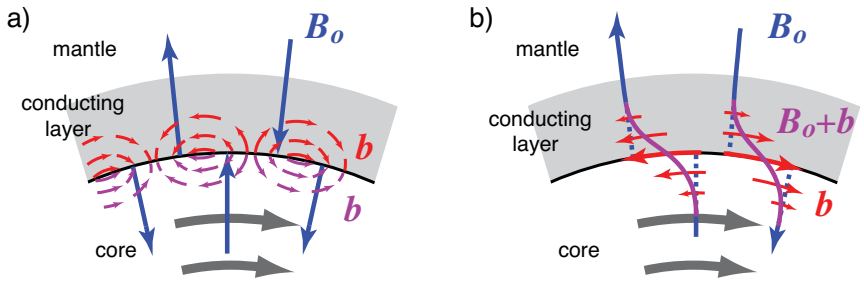

Figure 1. Perturbation of a background poloidal magnetic field $\mathbf{B_0}$ (blue) induced by a differential motion (depicted by grey arrows) between two conducting regions, here between the core and a conducting mantle. In (a), the secondary poloidal field results from the advection of the gradient of the background poloidal field on either side of the boundary. Only the radial part of the background poloidal field lines (blue) are shown. The poloidal perturbation $\mathbf{b}$ in the mantle (core), is shown by the red (purple) arrows. Note that, contrary to the mathematical definition we use in our study, the temporal change in $\mathbf{B_0}$ by the differential motion is not included in $\mathbf{b}$; as depicted here, $\mathbf{b}$ is discontinuous across the CMB, but in such a way that $\mathbf{B_0} + \mathbf{b}$ is continuous. In (b), stretching of the background poloidal field by the differential motion induces a toroidal field perturbation (red arrows). The stretched magnetic field lines (total field, $\mathbf{B_0} + \mathbf{b}$) are shown in purple.

and since $|b_r| \ll |\hat{\mathbf{r}} \times \mathbf{b}|$, to a very good approximation the EM torque can be written as

$$\mathbf{\Gamma} = \langle B_r \rangle \frac{r_b^3}{\mu} \int_\Omega (\hat{\mathbf{r}} \times \mathbf{b})\, \hat{B}_r \, d\Omega \,, \tag{55}$$

where we have decomposed B_r as

$$B_r = \langle B_r \rangle \hat{B}_r \,, \tag{56}$$

where $\langle B_r \rangle$ is the rms value and $\hat{B}_r$ is a non-dimensionalized magnetic field of rms value equal to one and with the same geometry as B_r.

Nutations involve the equatorial components of $\mathbf{\Gamma}$. By using the notation

$$\tilde{\Gamma} = \Gamma_x + \mathrm{i}\Gamma_y, \tag{57}$$

where the x-direction corresponds to $\phi = 0$, we can write (55) as

$$\tilde{\Gamma} = \langle B_r \rangle \frac{r_b^3}{\mu} \int_\Omega \left(\mathrm{i} b_\theta - b_\phi \cos\theta \right) e^{\mathrm{i}\phi} \hat{B}_r \, d\Omega \,. \tag{58}$$

Since both b_θ and b_ϕ have a toroidal and poloidal part, the torque can be separated into a toroidal ($\tilde{\Gamma}_T$) and poloidal ($\tilde{\Gamma}_P$) contribution which are, respectively,

$$\tilde{\Gamma}_T = \langle B_r \rangle \frac{r_b^3}{\mu} \int_\Omega \left(\frac{\mathrm{i}}{\sin\theta} \frac{\partial \mathcal{T}_b}{\partial \phi} + \cos\theta \frac{\partial \mathcal{T}_b}{\partial \theta} \right) e^{\mathrm{i}\phi} \hat{B}_r \, d\Omega \,, \tag{59}$$

$$\tilde{\Gamma}_P = \langle B_r \rangle \frac{r_b^3}{\mu} \int_\Omega \left(-\cot\theta \frac{\partial}{\partial \phi} \frac{\partial \mathcal{S}_b}{\partial r} + \mathrm{i} \frac{\partial}{\partial \theta} \frac{\partial \mathcal{S}_b}{\partial r} \right) e^{\mathrm{i}\phi} \hat{B}_r \, d\Omega \,, \tag{60}$$

where we have used the approximation $\frac{1}{r}\frac{\partial}{\partial r}(r\mathcal{S}_b) \approx \frac{\partial}{\partial r}\mathcal{S}_b$. Since $\frac{\partial}{\partial r}\mathcal{S}_b$ and $\mathcal{T}_b$ are of the same order of magnitude, we expect the poloidal and toroidal contributions to the torques to have similar magnitudes.

2.9.1 Toroidal torque

Integrating each term by parts, we can rewrite eq. (59) as

$$\tilde{\Gamma}_T = \langle B_r \rangle \frac{r_b^3}{\mu} \int_\Omega \mathcal{T}_b \, \mathcal{W}_T \, d\Omega \,, \tag{61}$$

where

$$\begin{aligned} \mathcal{W}_T &= -\frac{1}{\sin\theta} \left(\frac{\partial}{\partial \phi} \mathrm{i} \hat{B}_r e^{\mathrm{i}\phi} + \frac{\partial}{\partial \theta} \hat{B}_r \cos\theta \sin\theta \, e^{\mathrm{i}\phi} \right) , \\ &= \boldsymbol{\nabla}_1 \cdot (\hat{B}_r \boldsymbol{\nabla}_1 Y_1^{1*}) \,. \end{aligned} \tag{62}$$

Then, if we expand $\mathcal{W}_T$ as

$$\mathcal{W}_T = \sum_{l,m} w_{lm}^T \, Y_l^{m*} \,, \tag{63}$$

the coefficients w_{lm}^T are given by

$$w_{lm}^T = \frac{1}{N_{lm}} \int_\Omega Y_l^m \, \mathcal{W}_T \, d\Omega \,, \tag{64}$$

and can be calculated by spherical transforms for any $\hat{B}_r$.

Using the decomposition in (15), and orthogonality rules of spherical harmonics, the torque in (61) can be written in a convenient mathematical form,

$$\tilde{\Gamma}_T = \frac{\langle B_r \rangle}{2} \frac{r_b^3}{\mu} \sum_{l,m} N_{lm} \, w_{lm}^T \, t_{lm}^b \, e^{\mathrm{i}\omega t} \,, \tag{65}$$

where both w_{lm}^T and t_{lm}^b are evaluated at $r = r_b$. The evaluation of the toroidal torque then requires an evaluation of the coefficients t_{lm}^b of the toroidal perturbation.

2.9.2 Poloidal torque

Integrating each term once by parts, we can rewrite (60) as

$$\tilde{\Gamma}_P = \langle B_r \rangle \frac{r_b^3}{\mu} \int_\Omega \frac{\partial \mathcal{S}_b}{\partial r} \mathcal{W}_P \, d\Omega \,, \tag{66}$$

where

$$\begin{aligned} \mathcal{W}_P &= \cot\theta \frac{\partial}{\partial \phi} \hat{B}_r e^{\mathrm{i}\phi} - \frac{\mathrm{i} e^{\mathrm{i}\phi}}{\sin\theta} \frac{\partial}{\partial \theta} \hat{B}_r \sin\theta \,, \\ &= \left(\boldsymbol{\nabla}_1 \times Y_1^{1*} \hat{\mathbf{r}} \right) \cdot \boldsymbol{\nabla}_1 \hat{B}_r \,. \end{aligned} \tag{67}$$

If we expand $\mathcal{W}_P$ as

$$\mathcal{W}_P = \sum_{l,m} w_{lm}^P \, Y_l^{m*} \,, \tag{68}$$

the coefficients w_{lm}^P are given by

$$w_{lm}^P = -\frac{1}{N_{lm}} \int_\Omega Y_l^m \mathcal{W}_P \, d\Omega \,. \tag{69}$$

Using the decomposition (15), the torque in (66) can be written as

$$\tilde{\Gamma}_P = \frac{\langle B_r \rangle}{2} \frac{r_b^3}{\mu} \sum_{l,m} N_{lm} \, w_{lm}^P \, \dot{s}_{lm}^b \, e^{\mathrm{i}\omega t} \,, \tag{70}$$

where $\dot{s}_{lm}^b \equiv \frac{\partial}{\partial r} s_{lm}^b$, and where both w_{lm}^P and $\dot{s}_{lm}^b$ are evaluated at $r = r_b$.

2.10 Coupling constants

Because the differential nutation motion at both the ICB and CMB is small, the amplitude of the induced magnetic field is linearly proportional to the amplitude of the differential motion. The EM torque at the CMB by the mantle on the FOC, $\tilde{\Gamma}^{\mathrm{cmb}}$, can then be written in terms of a coupling constant K^{cmb} multiplied by their differential motion. The EM torque at the ICB by the FOC on the SIC, $\tilde{\Gamma}^{\mathrm{icb}}$, can be similarly written in terms of a coupling constant K^{icb}. The definition of these constants are (Mathews *et al.* 2002)

$$K^{\mathrm{cmb}} = \frac{\mathrm{i}\tilde{\Gamma}^{\mathrm{cmb}}}{\Omega_o A_f \tilde{\omega}_f} \tag{71a}$$

$$K^{\mathrm{icb}} = \frac{\mathrm{i}\tilde{\Gamma}^{\mathrm{icb}}}{\Omega_o A_s (\tilde{\omega}_s - \tilde{\omega}_f)}, \tag{71b}$$

where A_f and A_s are the mean equatorial moment of inertia of the FOC and SIC, respectively.

3 EM COUPLING IN THE WEAK FIELD LIMIT

When the amplitude of the background magnetic field is weaker than approximately 0.6 mT, the feedback from the Lorentz force generates a secondary flow which is negligible compared to the rigid-body nutation motion. In such a situation, the e.m.f. from the secondary flow can be neglected in the induction equation, a situation referred to as the 'weak field' approximation (Buffett *et al.* 2002).

3.1 Weak field solutions

To be explicit in the development of our solution, let us consider coupling at the ICB, though we retain the general variable r_b as the radius of this boundary. Within the fluid core ($r > r_b$), the

right-hand side of the toroidal (32a) and poloidal (32b) induction equations vanish and are then, respectively,

$$\left[\frac{\partial}{\partial t} - \eta\frac{\partial^2}{\partial r^2}\right]\mathcal{L}^2\mathcal{T}_b = 0\,, \tag{72a}$$

$$\left[\frac{\partial}{\partial t} - \eta\frac{\partial^2}{\partial r^2}\right]\mathcal{L}^2\frac{\partial\mathcal{S}_b}{\partial r} = 0\,. \tag{72b}$$

These are identical in form to the induction equations in the solid region given by (33a)–(33b).

Using the expansion (15), projecting on Y_l^{m*} and integrating over the unit sphere, we obtain a set of equations governing the evolution of each coefficients t_{lm}^b, $\dot{s}_{lm}^b$,

$$\mathrm{i}s|\omega|t_{lm}^b = \eta\frac{\partial^2}{\partial r^2}t_{lm}^b\,, \tag{73a}$$

$$\mathrm{i}s|\omega|\dot{s}_{lm}^b = \eta\frac{\partial^2}{\partial r^2}\dot{s}_{lm}^b\,, \tag{73b}$$

where we have defined

$$s = \frac{\omega}{|\omega|}\,. \tag{74}$$

A similar set of equations, though replacing η by η_s, applies for the coefficients in the solid region, $t_{lm}^{b(s)}$, $\dot{s}_{lm}^{b(s)}$. Solutions are

$$\left(t_{lm}^b,\ \dot{s}_{lm}^b\right) = \left(A_{lm}^T,\ A_{lm}^P\right)\exp\left[-\frac{(1+s\mathrm{i})}{\delta}(r-r_b)\right]\,, \tag{75a}$$

$$\left(t_{lm}^{b(s)},\ \dot{s}_{lm}^{b(s)}\right) = \left(A_{lm}^{T(s)},\ A_{lm}^{P(s)}\right)\exp\left[\frac{(1+s\mathrm{i})}{\delta_s}(r-r_b)\right]\,, \tag{75b}$$

where the sign in the exponential is chosen so that the perturbation decays away from the boundary, and where δ_s is the magnetic skin-depth in the solid region defined as

$$\delta_s = \sqrt{\frac{2\eta_s}{|\omega|}}\,. \tag{76}$$

The constants A_{lm} are determined by boundary conditions and solutions for the toroidal and poloidal coefficients, at $r = r_b$, are

$$t_{lm}^b(r_b) = -\frac{\langle B_r\rangle r_b\Delta\hat{\omega}_b F}{l(l+1)}\,w_{lm}^{T\,*}\,, \tag{77a}$$

$$\dot{s}_{lm}^b(r_b) = -\frac{\langle B_r\rangle r_b\Delta\hat{\omega}_b F}{l(l+1)}\,w_{lm}^{P\,*}\,, \tag{77b}$$

where

$$F = \frac{(1-s\mathrm{i})}{2}\left(\frac{\eta}{\delta}+\frac{\eta_s}{\delta_s}\right)^{-1}\,. \tag{78}$$

The toroidal and poloidal torque can be written in the form

$$\tilde{\Gamma}_T = -\frac{1}{2}\frac{r_b^4}{\mu}\langle B_r\rangle^2\,F\,C_T\,\Delta\hat{\omega}_b\,e^{\mathrm{i}\omega t}\,, \tag{79a}$$

$$\tilde{\Gamma}_P = -\frac{1}{2}\frac{r_b^4}{\mu}\langle B_r\rangle^2\,F\,C_P\,\Delta\hat{\omega}_b\,e^{\mathrm{i}\omega t}\,, \tag{79b}$$

where

$$C_T = \sum_{l,m}\frac{N_{lm}}{l(l+1)}\left|w_{lm}^T\right|^2\,, \tag{80a}$$

$$C_P = \sum_{l,m}\frac{N_{lm}}{l(l+1)}\left|w_{lm}^P\right|^2\,, \tag{80b}$$

and where $|\cdot|$ denotes the complex modulus. C_T and C_P can be evaluated for any model of $\hat{B}_r$ at the boundary.

It follows that the toroidal and poloidal parts of the coupling constants K^{cmb} and K^{icb} defined in (71) are given by the general expressions

$$K_T^b = -\frac{(s+\mathrm{i})}{4}\langle B_r\rangle^2\gamma\,C_T\,, \tag{81a}$$

$$K_P^b = -\frac{(s+\mathrm{i})}{4}\langle B_r\rangle^2\gamma\,C_P\,, \tag{81b}$$

where

$$\gamma = \frac{r_b^4}{\Omega_o A_b}\left(\frac{1}{\sigma\delta}+\frac{1}{\sigma_s\delta_s}\right)^{-1}\,. \tag{82}$$

We note that these expressions are valid at both the CMB (where $r_b = r_f$ and $A_b = A_f$) and the ICB ($r_b = r_s$ and $A_b = A_s$). In the weak field limit, the amplitude of the torque, and thus the coupling constants, increase quadratically with an increase in the radial magnetic field strength.

3.2 Comparison with previous model

As we noted in Sections 2.5 and 2.6, our induction and momentum equations are equivalent to those used by Buffett *et al.* (2002). We also use the same boundary conditions and therefore, our model should produce equivalent results. This is true for any choice of background magnetic field strength and geometry. Since relatively simple analytical solutions exist in the weak field limit, we can show this equivalence explicitly on the basis of two simple background field configurations, namely, for a uniform radial field and an axial dipole field. Although a uniform field is not physically realistic, since it is the square of B_r that enters in the torque, it can be thought of as the mean rms value of a realistic global B_r field that includes many small scale features.

When B_r is axisymmetric, Buffett *et al.* (2002) showed that the EM torque can be expressed, in our notation, as

$$\tilde{\Gamma} = -\frac{\pi r_b^4 F}{\mu}\Delta\hat{\omega}_b\,e^{\mathrm{i}\omega t}\int B_r^2(1+\cos^2\theta)\sin\theta\,d\theta\,. \tag{83}$$

Values for $\tilde{\Gamma}$ and K^b can be computed on the basis of this expression. For the case of a uniform field $B_r = \langle B_r\rangle$, eq. (83) gives

$$\tilde{\Gamma} = -\frac{8\pi}{3}\frac{r_b^4 F\langle B_r\rangle^2}{\mu}\,\Delta\hat{\omega}_b\,e^{\mathrm{i}\omega t}\,, \tag{84}$$

and the coupling constant is

$$K^b = -\frac{4\pi}{3}\gamma(s+\mathrm{i})\langle B_r\rangle^2\,. \tag{85}$$

For an axial dipole, defined by $B_r = \sqrt{3}\langle B_r^d\rangle\cos\theta$, where $\langle B_r^d\rangle$ denotes the rms amplitude of the radial part, eq. (83) gives

$$\tilde{\Gamma} = -\frac{16\pi}{5}\frac{r_b^4 F\langle B_r^d\rangle^2}{\mu}\,\Delta\hat{\omega}_b\,e^{\mathrm{i}\omega t}\,, \tag{86}$$

and

$$K^b = -\frac{8\pi}{5}\gamma(s+\mathrm{i})\langle B_r^d\rangle^2\,. \tag{87}$$

We now show that our global model gives the same result, and in the process we also determine the relative contribution of the

toroidal and poloidal parts to the total torque. In the case of a uniform field $B_r = \langle B_r \rangle$, and thus $\hat{B}_r = 1$ in eq. (62), the only non-zero coefficient w^T_{lm} is w^T_{11} which equals

$$w^T_{11} = -2\,, \tag{88}$$

and thus, from (77a),

$$t^b_{11} = r_b\, F\, \langle B_r \rangle\, \Delta\hat{\omega}_b\,. \tag{89}$$

For such a simple field, the coefficient C_T equals

$$C_T = \frac{16\pi}{3}\,, \tag{90}$$

so the toroidal coupling constant is equal to

$$K^b_T = -\frac{4\pi}{3}\gamma(s+\mathrm{i})\langle B_r\rangle^2\,. \tag{91}$$

Since the source of the poloidal perturbation requires lateral gradients of B_r, when $B_r = \langle B_r \rangle$ there is no poloidal perturbation, so $C_P = K^b_P = 0$; the torque results solely from the toroidal perturbation. We thus get a total K^b of

$$K^b = K^b_T + K^b_P = -\frac{4\pi}{3}\gamma(s+\mathrm{i})\langle B_r\rangle^2, \tag{92}$$

which is equivalent to eq. (85).

For an axial dipole field of rms strength $\langle B^d_r \rangle$ and using $\hat{B}_r = \sqrt{3}\cos\theta$ in (62), we find that

$$\mathcal{W}_T = -\sqrt{3}\, P^1_2\, e^{\mathrm{i}\phi}\,, \tag{93}$$

and thus that the only non-zero w^T_{lm} coefficient is w^T_{21} which equals

$$w^T_{21} = -\sqrt{3}\,. \tag{94}$$

The toroidal magnetic field perturbation is then expressed by a spherical harmonic of degree 2 order 1 with coefficient

$$t^b_{21} = \frac{\sqrt{3}}{6} r_b\, F\left\langle B^d_r \right\rangle \Delta\hat{\omega}_b\, e^{\mathrm{i}\omega t}\,. \tag{95}$$

Using (94), we get

$$C_T = \frac{12\pi}{5}\,, \tag{96}$$

and the toroidal part of the coupling constant is

$$K^b_T = -\frac{3\pi}{5}\gamma(s+\mathrm{i})\left\langle B^d_r \right\rangle^2\,. \tag{97}$$

To evaluate the poloidal part of the torque, using (67) one can show that

$$\mathcal{W}_P = -\mathrm{i}\sqrt{3}\, P^1_1\, e^{i\phi}\,, \tag{98}$$

and thus that

$$w^P_{11} = -\mathrm{i}\sqrt{3} \tag{99}$$

and all other coefficients w^P_{lm} are zero. It follows that

$$\dot{s}^b_{11} = \mathrm{i}\frac{\sqrt{3}}{2} r_b\, F\left\langle B^d_r \right\rangle \Delta\hat{\omega}_b\, e^{\mathrm{i}\omega t}\,, \tag{100}$$

$$C_P = 4\pi\,, \tag{101}$$

and

$$K^b_P = -\pi(\mathrm{i}+s)\gamma\left\langle B^d_r \right\rangle^2\,. \tag{102}$$

Comparing (97) and (102) shows that, for the case of an axial dipole, the poloidal torque is larger than the toroidal torque by a factor 5/3. Moreover, summing the toroidal and poloidal contributions of the coupling constants, we get

$$K^b = K^b_T + K^b_P = -\frac{8\pi}{5}\gamma(s+\mathrm{i})\left\langle B^d_r \right\rangle^2\,, \tag{103}$$

which is equivalent to eq. (87) (and also equivalent to the results of Greff-Lefftz & Legros 1999).

3.3 The different nature of the poloidal and toroidal torque

Our global model allows us to separate the EM torque into its poloidal and toroidal contribution. For the dipole case developed in the previous section, they each contribute to the EM torque by approximately the same amount. Of course, it is the total torque that is important, and for the examples of the previous section, knowing the individual contribution of the poloidal and toroidal torque does not appear to be necessary. However, this separation can be important for specific radial profiles of the conductivity on the solid side, a fact that we illustrate with the following example.

Let us imagine that the conducting mantle (of electrical conductivity σ_s) is separated from the core by an insulating layer of thickness Δ. The presence of this layer does not allow electrical currents from the core to communicate with those in the conducting mantle above. Since all currents must vanish at the CMB, a differential rotation of the core does not produce an EM stress at the CMB. However, it does produce an EM stress on the bottom of the conducting region of the mantle: an EM torque is applied on the mantle. Assuming a uniform conductivity structure, the nature of this torque is purely poloidal. To understand this, we must recall that a change in toroidal field $\mathcal{T}_b$ within the conducting mantle can only result from diffusion of a toroidal source at its boundary (see eq. 33a). Since $\mathcal{T}_b = 0$ in the insulating region (because it requires a poloidal electrical current), no toroidal field can be transferred to the conducting mantle. However, a source of poloidal field does exist at the bottom of the conducting region: the potential poloidal field $\mathcal{S}_b$ caused by the lateral displacement of background poloidal field structure generated in the core and instantly diffusing through the insulating region. The condition on $\mathcal{S}_b$ in the insulating region is $\partial^2\mathcal{S}_b/\partial r^2 = 0$, therefore $\partial\mathcal{S}_b/\partial r$ must be constant, but does not vanish. The solution of the poloidal perturbation and EM torque are equivalent to the expressions given by eqs. (77b) and (79b), respectively, though r_b must be replaced by $r_b + \Delta$, $\langle B_r \rangle$ now represents the field amplitude at this radius, and $F = (1 - s\mathrm{i})\delta_s\mu\sigma_s/2$.

Another illustrative mantle conductivity scenario is one where a thin insulating layer exists close to the CMB, within the skin-depth of the propagation of the induced magnetic field (Fig. 2). The toroidal perturbation would not penetrate past this layer, whilst this would not present a problem for the poloidal perturbation. The restriction on the toroidal perturbation would reduce the amplitude of the toroidal torque significantly, but the poloidal torque would remain virtually unchanged.

Though very contrived, the above conductivity scenarios illustrate the different nature of the poloidal and toroidal torque. In such cases, the separation of these two contribution is necessary. Such scenarios cannot be captured by 'local' EM models in their current form (though they could be extended to do so). While these scenarios may not be applicable to Earth, they may apply to other planetary bodies.

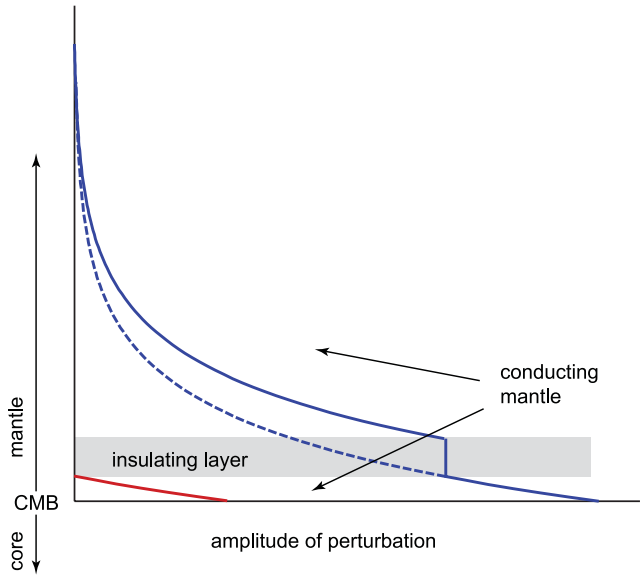

Figure 2. Illustration of the effect of a thin insulating layer (of thickness $\Delta < \delta_s$) on the toroidal ($\mathcal{T}_b$) and poloidal ($\partial\mathcal{S}_b/\partial r$) perturbation in the mantle. As a reference, the solution of both $\mathcal{T}_b$ and $\partial\mathcal{S}_b/\partial r$ in the absence of the insulating layer is depicted by the dashed blue line. (For the purpose of illustration, these solutions are simple exponentially decaying functions.) Within the insulating region, $\mathcal{T}_b = 0$ and $\partial\mathcal{S}_b/\partial r =$ cst. Thus, the amplitude of $\mathcal{T}_b$ at the CMB is significantly reduced (red line) while the solution of $\partial\mathcal{S}_b/\partial r$ (solid blue line) is identical except displaced in radius above the conducting region.

4 EM COUPLING IN THE 'STRONG FIELD' REGIME

When the feedback from the Lorentz force contributes to a significant departure of the core motion from that of a uniform rigid body rotation, the induction and momentum equations must be solved jointly for the flow and magnetic field perturbations. The magnetic field perturbation no longer obeys a diffusion equation profile in radius; instead, the e.m.f. from the induced flow allows for MC waves to be part of the solutions. This alters the amplitude and geometry of the induced magnetic field significantly, and therefore the EM torque is also altered. We now show how the EM torque in this 'strong field' regime can be computed using our global formalism.

4.1 Description of the model

Using eqs (15) and (17), the toroidal and poloidal induction equations (eq. 32) in the fluid core can be written as

$$\sum_{lm} l(l+1)\left(\mathrm{i}\omega - \eta\frac{\partial^2}{\partial r^2}\right) t^b_{lm} = -\langle B_r\rangle \sum_{l'm'}\left[\left(\mathcal{W}_T^{l'm'}\right)^* \frac{\partial}{\partial r} t^f_{l'm'} - \left(\mathcal{W}_P^{l'm'}\right)^* \frac{\partial}{\partial r}\dot{s}^f_{l'm'}\right], \quad (104a)$$

$$\sum_{lm} l(l+1)\left(\mathrm{i}\omega - \eta\frac{\partial^2}{\partial r^2}\right) \dot{s}^b_{lm} = -\langle B_r\rangle \sum_{l'm'}\left[\left(\mathcal{W}_P^{l'm'}\right)^* \frac{\partial}{\partial r} t^f_{l'm'} + \left(\mathcal{W}_T^{l'm'}\right)^* \frac{\partial}{\partial r}\dot{s}^f_{l'm'}\right], \quad (104b)$$

where

$$\mathcal{W}_T^{lm} = \boldsymbol{\nabla}_1\cdot(\hat{B}_r\boldsymbol{\nabla}_1 Y_l^{m*}), \quad (105a)$$

$$\mathcal{W}_P^{lm} = \left(\boldsymbol{\nabla}_1\times Y_l^{m*}\hat{\mathbf{r}}\right)\cdot\boldsymbol{\nabla}_1\hat{B}_r\,. \quad (105b)$$

Note that $\mathcal{W}_T^{lm}$ and $\mathcal{W}_P^{lm}$ are more general functions than the functions $\mathcal{W}_T$ and $\mathcal{W}_P$ defined in eqs. (62) and (67), respectively, and

$$\mathcal{W}_T^{11} = \mathcal{W}_T \qquad \mathcal{W}_P^{11} = \mathcal{W}_P\,. \quad (106)$$

Further, we can expand $\mathcal{W}_T^{lm}$ as

$$\mathcal{W}_T^{lm} = \sum_{l',m'} w^{Tlm}_{l'm'}\, Y_{l'}^{m'*}, \quad (107)$$

with

$$w^{Tlm}_{l'm'} = \frac{1}{N_{l'm'}}\int_\Omega Y_{l'}^{m'}\left[\boldsymbol{\nabla}_1\cdot(\hat{B}_r\boldsymbol{\nabla}_1 Y_l^{m*})\right] d\Omega\,. \quad (108)$$

Coefficients $w^{Plm}_{l'm'}$ are similarly defined, and can be calculated by spherical transforms for any magnetic field model of $\hat{B}_r$.

Projecting eq. (104) on Y_l^{m*} and integrating over the unit sphere, we obtain a set of equations governing the evolution of each coefficients t^b_{lm} and $\dot{s}^b_{lm}$,

$$l(l+1)\left(\mathrm{i}\omega - \eta\frac{\partial^2}{\partial r^2}\right) t^b_{lm} = -\langle B_r\rangle \sum_{l'm'}\left[\left(w^{Tl'm'}_{lm}\right)^* \frac{\partial}{\partial r} t^f_{l'm'} - \left(w^{Pl'm'}_{lm}\right)^* \frac{\partial}{\partial r}\dot{s}^f_{l'm'}\right], \quad (109a)$$

$$l(l+1)\left(\mathrm{i}\omega - \eta\frac{\partial^2}{\partial r^2}\right) \dot{s}^b_{lm} = -\langle B_r\rangle \sum_{l'm'}\left[\left(w^{Pl'm'}_{lm}\right)^* \frac{\partial}{\partial r} t^f_{l'm'} + \left(w^{Tl'm'}_{lm}\right)^* \frac{\partial}{\partial r}\dot{s}^f_{l'm'}\right]. \quad (109b)$$

The toroidal and poloidal momentum equations (eq. 39) can be expanded in a similar way, leading to dynamic equations for the evolution of the coefficients t^f_{lm} and $\dot{s}^f_{lm}$,

$$\left(\mathrm{i}\,l(l+1)\frac{\omega}{\Omega_o} + 2\mathrm{i}m\right) t^f_{lm} - 2c^m_l\dot{s}^f_{l-1,m} - 2c^m_{l+1}\dot{s}^f_{l+1,m} = -\frac{\langle B_r\rangle}{\rho\mu\Omega_o}\sum_{l'm'}\left[\left(w^{Tl'm'}_{lm}\right)^* \frac{\partial}{\partial r} t^b_{l'm'} - \left(w^{Pl'm'}_{lm}\right)^* \frac{\partial}{\partial r}\dot{s}^b_{l'm'}\right], \quad (110a)$$

$$\left(\mathrm{i}\,l(l+1)\frac{\omega}{\Omega_o} + 2\mathrm{i}m\right) \dot{s}^f_{lm} + 2c^m_l t^f_{l-1,m} + 2c^m_{l+1} t^f_{l+1,m} = -\frac{\langle B_r\rangle}{\rho\mu\Omega_o}\sum_{l'm'}\left[\left(w^{Pl'm'}_{lm}\right)^* \frac{\partial}{\partial r} t^b_{l'm'} + \left(w^{Tl'm'}_{lm}\right)^* \frac{\partial}{\partial r}\dot{s}^b_{l'm'}\right], \quad (110b)$$

where

$$c^m_l = (l+1)(l-1)\sqrt{\frac{(l+m)(l-m)}{(2l+1)(2l-1)}}\,. \quad (111)$$

The coupled ODE's formed by eqs (109)–(110) can be expressed in a more concise form by taking advantage of the symmetries of the system. Let us define the vectors $\mathbf{t}_\mathbf{f}^{(\mathbf{s})}$ and $\mathbf{t}_\mathbf{f}^{(\mathbf{a})}$, containing the coefficients of the harmonics of the flow that are, respectively, symmetric and antisymmetric about the equator. The ordering of the coefficients is as follows: we first take the sequence of coefficients with harmonic order $m = 0$ (ordered in increasing harmonic degrees l), then the sequence of coefficients with $m = 1$, followed by those with $m = -1$, then $m = 2$, $m = -2$, etc.,

$$\mathbf{t}_\mathbf{f}^{(\mathbf{s})} = \left(t^f_{10}, \dot{s}^f_{20}, t^f_{30}, \ldots \dot{s}^f_{11}, t^f_{21}, \dot{s}^f_{31}, \ldots \dot{s}^f_{1-1}, t^f_{2-1}, \dot{s}^f_{3-1}, \ldots \dot{s}^f_{22}, t^f_{32}, \ldots \dot{s}^f_{2-2}, t^f_{3-2}, \ldots\right), \quad (112a)$$

$$\mathbf{t}_\mathbf{f}^{(\mathbf{a})} = \left(\dot{s}_{10}^f, t_{20}^f, \dot{s}_{30}^f, \ \ldots\ t_{11}^f, \dot{s}_{21}^f, t_{31}^f, \ \ldots\ t_{1-1}^f, \dot{s}_{2-1}^f, t_{3-1}^f, \right.$$
$$\left. \ldots\ t_{22}^f, \dot{s}_{32}^f, \ \ldots\ t_{2-2}^f, \dot{s}_{3-2}^f, \ \ldots\right). \tag{112b}$$

Vectors of symmetric and antisymmetric magnetic field coefficients, $\mathbf{t}_\mathbf{b}^{(\mathbf{s})}$ and $\mathbf{t}_\mathbf{b}^{(\mathbf{a})}$, are defined identically. Using this notation, we can write the momentum eqs (110a and b) in matrix form as

$$\mathsf{A}_f \cdot \mathbf{t}_\mathbf{f} = -\frac{\langle B_r \rangle}{\rho\mu\Omega_o}\, \mathsf{B} \cdot \frac{\partial}{\partial r}\mathbf{t}_\mathbf{b}\,, \tag{113}$$

where

$$\mathbf{t}_\mathbf{f} = \begin{bmatrix} \mathbf{t}_\mathbf{f}^{(\mathbf{a})} \\ \mathbf{t}_\mathbf{f}^{(\mathbf{s})} \end{bmatrix}, \qquad \mathbf{t}_\mathbf{b} = \begin{bmatrix} \mathbf{t}_\mathbf{b}^{(\mathbf{a})} \\ \mathbf{t}_\mathbf{b}^{(\mathbf{s})} \end{bmatrix}. \tag{114}$$

The advantage of using such a vector ordering is that matrix A_f is then tri-diagonal (e.g. Hollerbach & Kerswell 1995) and easily invertible. Further, when B_r is purely symmetric about the equator, the interaction between the (antisymmetric) nutation flow and B_r produces a purely antisymmetric magnetic field perturbation, so $\mathbf{t}_\mathbf{b}^{(\mathbf{s})} = \mathbf{0}$. The interaction between the purely antisymmetric $\mathbf{t}_\mathrm{b}$ and B_r (that enters matrix B) described by eq. (113) leads to a purely antisymmetric flow perturbation, so $\mathbf{t}_\mathbf{f}^{(\mathbf{s})} = \mathbf{0}$. The number of elements in the solution vector can thus be reduced by a factor 2. Similarly, when B_r is purely antisymmetric, $\mathbf{t}_\mathbf{b}^{(\mathbf{a})} = \mathbf{0}$ and $\mathbf{t}_\mathbf{f}^{(\mathbf{s})} = \mathbf{0}$.

The induction equation, in matrix form, is

$$\left(\mathrm{i}\omega - \eta\frac{\partial^2}{\partial r^2}\right)\mathcal{L}^2\mathbf{t}_\mathbf{b} = -\langle B_r\rangle\, \mathsf{B} \cdot \frac{\partial}{\partial r}\mathbf{t}_\mathbf{f}\,. \tag{115}$$

Inserting (113) in (115), we obtain

$$\left(\mathrm{i}\omega - \eta\frac{\partial^2}{\partial r^2}\right)\mathcal{L}^2\mathbf{t}_\mathbf{b} = \eta\Lambda\, \mathsf{D} \cdot \frac{\partial^2}{\partial r^2}\mathbf{t}_\mathbf{b}\,, \tag{116}$$

where Λ is the Elsasser number

$$\Lambda = \frac{\langle B_r\rangle^2\,\sigma}{\rho\Omega_\mathrm{o}}\,, \tag{117}$$

and where

$$\mathsf{D} = \mathsf{B} \cdot \mathsf{A}_f^{-1} \cdot \mathsf{B}\,. \tag{118}$$

The set of equations represented by eq. (116) are coupled ODE's in radius. Solutions are exponential functions in r (normal modes) in the form of

$$\mathbf{t}_\mathbf{b}(r) = \mathbf{t}_\mathbf{b}^+ \exp[\lambda(r - r_b)]\,, \tag{119}$$

where $\mathbf{t}_\mathbf{b}^+ = \mathbf{t}_\mathbf{b}(r_b)$. Substituting this ansatz in eq. (116),

$$\left(\mathrm{i}\omega\mathcal{L}^2 - \eta\lambda^2\mathcal{L}^2\right)\mathbf{t}_\mathbf{b}^+ = \eta\Lambda\,\lambda^2\,\mathsf{D} \cdot \mathbf{t}_\mathbf{b}^+\,. \tag{120}$$

This system can be written in the form of an eigenvalue problem

$$\mathsf{A} \cdot \mathbf{x} = \lambda^{-2}\mathbf{x}\,. \tag{121}$$

Two families of eigenvalues are found: those which have $\mathrm{Re}(\lambda) > 0$ and those with $\mathrm{Re}(\lambda) < 0$, corresponding, respectively, to exponentially growing and decaying perturbations away from the ICB (and vice versa if r_b is the CMB). Exponentially growing solutions are eliminated by the condition that the induced magnetic field should vanish far away from the boundary. The imaginary part of λ corresponds to oscillations propagating in the radial direction. When $\Lambda \ll 1$, we retrieve the set of decoupled diffusion equation for each of the coefficient of the induced magnetic field, and so we recover the weak field solutions of the previous section. When $\Lambda \approx 1$, the normal modes contain both oscillatory and decaying parts. $\Lambda \approx 1$ corresponds to $B_r = 1.8$ mT so we expect that these modes are relevant for coupling at the ICB.

The solution in the fluid can then be expressed as a sum of the normal modes

$$\mathbf{t}_\mathbf{b} = \sum_j c_j(\mathbf{t}_\mathbf{b}^+)_j \exp[\lambda_j(r - r_b)]\,, \tag{122}$$

where the λ_j are the individual eigenvalues and $(\mathbf{t}_b^+)_j$ the associated eigenvectors. The coefficients c_j are multiplying factors which are determined by boundary conditions.

On the solid side of the boundary, solutions are identical to those found in the weak field case. To cast these solutions in the same form as those in the fluid, we write

$$\mathbf{t}_\mathbf{b}^\mathbf{s}(r) = \mathbf{t}_\mathbf{b}^- \exp[\lambda_s(r - r_b)]\,, \tag{123}$$

where $\mathbf{t}_\mathbf{b}^- = \mathbf{t}_\mathbf{b}^\mathbf{s}(r_b)$, and the induction equation is simply

$$\left(\mathrm{i}\omega - \eta_s\lambda_s^2\right)\mathbf{t}_\mathbf{b}^- = \mathbf{0}\,. \tag{124}$$

A solution to this eigenvalue problem is simply a matrix of column eigenvectors $(\mathbf{t}_\mathbf{b}^-)_j$ equal to the identity matrix, all sharing the same (degenerate) eigenvalue

$$\lambda_s = \frac{(1 + s\mathrm{i})}{\delta_s}\,, \tag{125}$$

where s is defined in eq. (74). The solution is expressed as the sum of these modes

$$\mathbf{t}_\mathbf{b}^\mathbf{s} = \sum_j c_j^s\,(\mathbf{t}_\mathbf{b}^-)_j\, \exp[\lambda_s(r - r_b)]\,. \tag{126}$$

The boundary conditions in eqs. (46–47) imply that

$$\sum_j c_j(\mathbf{t}_\mathbf{b}^+)_j = \sum_j c_j^s(\mathbf{t}_\mathbf{b}^-)_j\,, \tag{127}$$

and the conditions in eqs. (50–51) imply

$$\eta\sum_j c_j\lambda_j(\mathcal{L}^2 + \Lambda\mathsf{D})(\mathbf{t}_\mathbf{b}^+)_j - \eta_s\sum_j c_j^s\lambda_s\mathcal{L}^2(\mathbf{t}_\mathbf{b}^-)_j = -\langle B_r\rangle\mathsf{B} \cdot \mathbf{t}_\mathbf{n}, \tag{128}$$

where the vector $\mathbf{t}_\mathrm{n}$ contains the differential nutation motion. These conditions uniquely determine all coefficients c_j and c_j^s for a given $\mathbf{t}_\mathrm{n}$. Solutions of $\mathbf{t}_\mathrm{b}$ as given by eq. (122) and evaluated at $r = r_b$ can then be substituted in eqs. (65) and (70) to obtain, respectively, the toroidal and poloidal contributions to the torque.

4.2 Strong field solutions

We now present solutions of our model. To be specific we consider EM coupling at the ICB. For all the calculations presented below, we have used $\sigma = \sigma_s = 5 \times 10^5$ S m^{-1}, $r_b = r_s = 1221.5$ km, $A_b = A_s = 5.8531 \times 10^{34}$ kg m^2 and a density of the fluid core at the ICB of 1.217×10^4 kg m^{-3}. In Fig. 3 we show how the coefficients t_{lm}^b and $\dot{s}_{lm}^b$ of the magnetic field perturbation vary as a function of radial distance away from the ICB in the fluid core. These solutions are computed on the basis of a background magnetic field described by an axial dipole of the form $B_r = \sqrt{3}\langle B_r^d\rangle\cos\theta$. We first show a solution approaching the weak field limit, with $\langle B_r^d\rangle = 0.1$ mT (Figs 3a and b). With such a small rms radial magnetic field, the feedback from the Lorentz force is unimportant and the magnetic field perturbation is dominated by the coefficients t_{21}^b and $\dot{s}_{11}^b$, as expected based on the weak field limit solutions (see eqs. 95 and 100). Other coefficients that are not identically zero have amplitudes that are smaller by at least two orders of magnitude. The radial variation follows the exponentially decaying diffusion profile described by eq. (75), propagating in the fluid core only as far as a

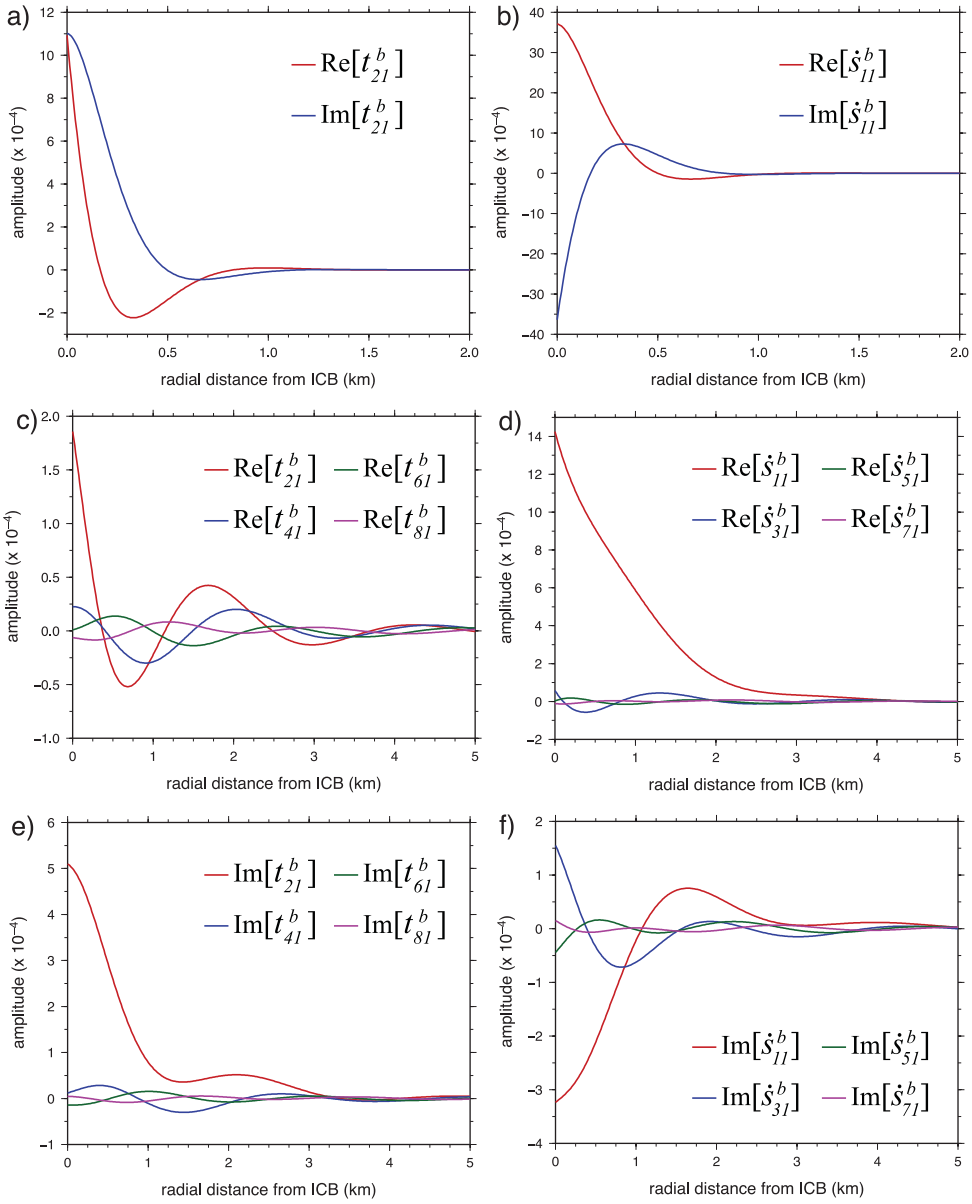

Figure 3. Spherical harmonic coefficients of the magnetic field perturbation in the fluid core as a function of radial distance above the ICB, when the background magnetic field is an axial dipole of the form $B_r = \sqrt{3}\langle B_r^d\rangle \cos\theta$, with (a, b) $\langle B_r^d\rangle = 0.1$ mT; (c, d, e, f) $\langle B_r^d\rangle = 4$ mT. For all plots, the coefficients amplitude have been divided by $\langle B_r^d\rangle$ and are dimensionless. The nutation flow amplitude used in the computation is $\Delta\hat{\omega}_b = \Omega_o \times 10^{-6}$.

distance of the order of the magnetic skin-depth (of $\delta = 0.209$ km for the chosen parameters).

In the strong field regime, the feedback between the flow perturbations and the magnetic field results in a magnetic field perturbation that comprises more harmonics. With an axial dipole background radial field, non-zero harmonics coefficients are restricted to t^b_{n1} with $n =$ even, and $\dot{s}^b_{n1}$ with $n =$ odd. The radial variation of the first few of these coefficients are shown in Figs 3(c)–(f), for the case $\langle B_r^d\rangle = 4$ mT. Interaction between the flow and magnetic field produce MC waves that are initiated at the ICB and propagate to a much greater depth in the fluid core than the magnetic skin depth.

While the magnetic field perturbation in the weak field limit is restricted to only one toroidal and one poloidal harmonics, and therefore has a very simple structure, the contribution of many harmonics in the strong field regime solution creates a more complex magnetic field morphology. This is illustrated in Figs 4(a) and (b), where we show the solution of the magnetic field perturbation as a function of geographic position on the spherical surface of the ICB, for $\langle B_r^d\rangle = 0.1$ mT and 4 mT, respectively. The associated flow perturbation at the ICB, in the strong field regime, is shown in Fig. 4(c). These solutions correspond to a snapshot in time when, in the frame of the FOC, the inner core rotation vector is directed towards longitude $= 0$; as a function of time, the whole solution moves westward with a period of 1 day. Note that the horizontal flow pattern in Fig. 4(c) follows closely the motion of the rigid nutation motion of the inner core (except near the equator), with almost the same amplitude. This reflects the magnetic entrainment of the flow near the ICB by the differentially rotating inner core. This flow entrainment reduces the overall stretching and differential advection of the background radial magnetic field: this is the reason why the magnetic perturbation amplitude, when normalized by $\langle B_r^d\rangle$, is weaker in the strong field regime than in the weak field limit, as

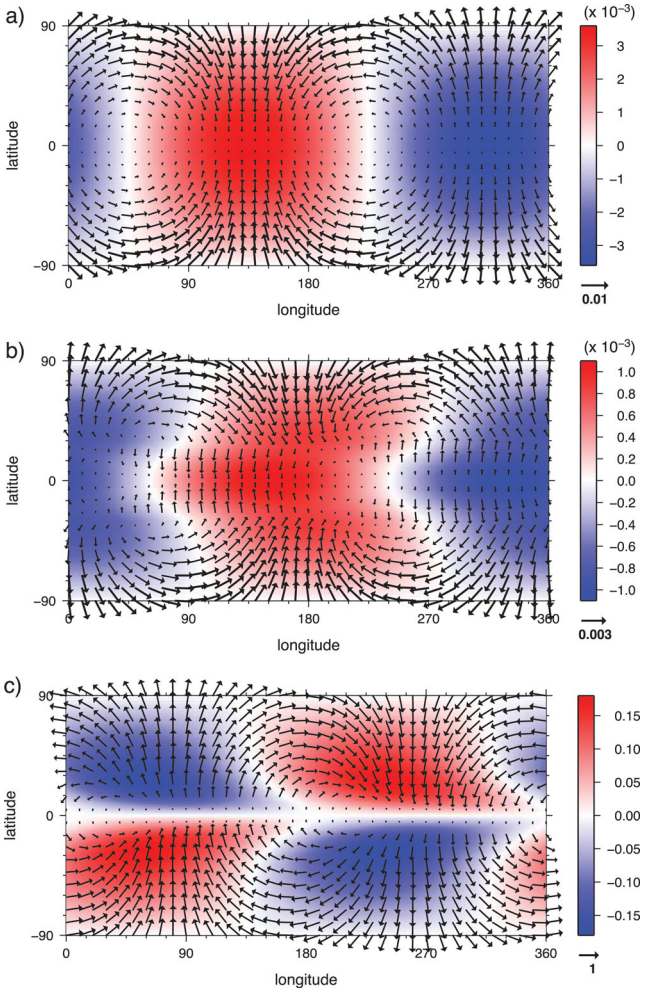

Figure 4. Magnetic field perturbation as a function of geographic position at the ICB for an assumed axial dipole background radial magnetic field of the form $B_r = \sqrt{3}\langle B_r^d\rangle \cos\theta$, (a) in the weak field limit with $\langle B_r^d\rangle = 0.1$ mT and (b) in the strong field regime with $\langle B_r^d\rangle = 4$ mT. Arrows show the magnetic field components parallel to the ICB and colours show the radial derivative of the poloidal scalar, $\partial \mathcal{S}_b/\partial r$. Amplitudes have been divided by $\langle B_r^d\rangle$ and are dimensionless. The nutation flow amplitude used in the computation is $\Delta\hat{\omega}_b = \Omega_o \times 10^{-6}$. In (c), we show the flow perturbation for $\langle B_r^d\rangle = 4$ mT. Arrows show the flow components parallel to the ICB and colours show the radial derivative of the poloidal scalar, $\partial \mathcal{S}_f/\partial r$. Amplitudes have been divided by $r_b \Delta\hat{\omega}_b$ and are dimensionless; they represent the relative amplitude of the flow perturbation compared to the differential rigid nutation motion at the ICB.

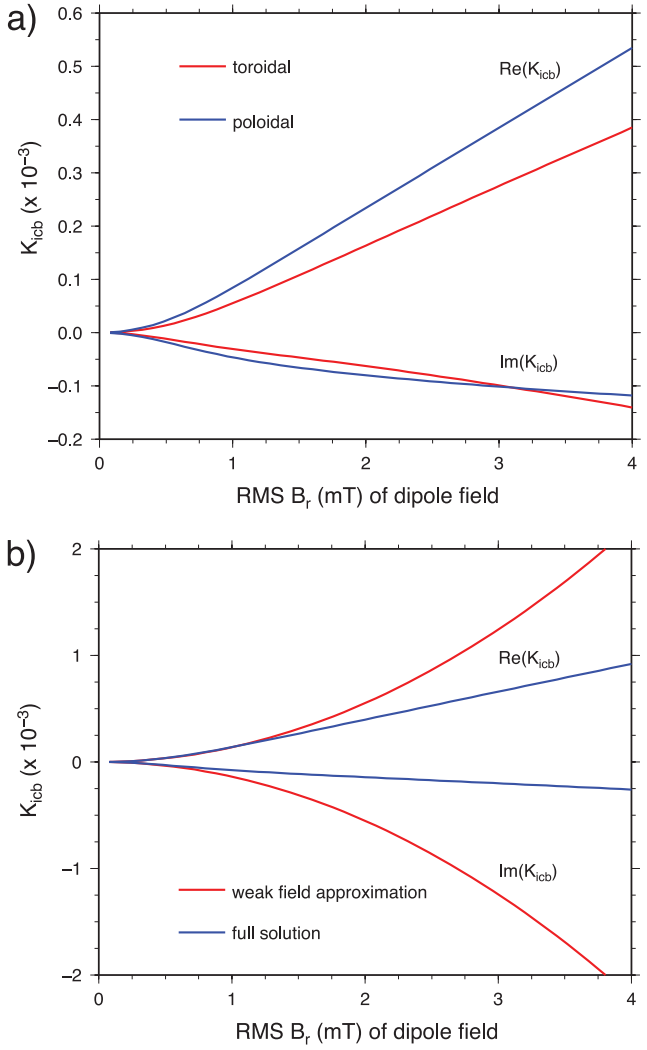

Figure 5. (a) The toroidal and poloidal parts of $K^{\rm icb}$ as a function of the rms amplitude of an axial dipole background radial field. (b) $K^{\rm icb}$ versus rms amplitude of an axial dipole background field.

illustrated in Figs 3, 4(a) and (b). The reason for the much weaker flow at low latitude is because the radial part of the axial dipole background field vanishes at the equator. Flows tangential to the ICB must then vanish at the equator and, because our flows are divergence free, this forces a strong flow in the radial direction in the vicinity of the equator.

In Fig. 5(a), we show how the poloidal and toroidal parts of $K^{\rm icb}$ change as a function of the rms amplitude of the radial field $\langle B_r^d\rangle$, again for an axial dipole background radial field. The change in the sum of these two contributions (i.e. the total $K^{\rm icb}$) as a function of $\langle B_r^d\rangle$ is shown in Fig. 5(b), where we also show a comparison with the solution computed in the weak-field limit. The result in Fig. 5(b) is identical to that obtained with the 'local' model of Buffett *et al.* (2002), and shows how the feedback from the Lorentz force on core flows significantly alters the EM torque when $\langle B_r^d\rangle$ is larger than approximately 0.8 mT. Past this point, the strength of the coupling no longer increases quadratically with $\langle B_r^d\rangle$ and the real and imaginary parts no longer have equal magnitudes. The effective reduction of the EM coupling strength is caused by the entrainment of the flow in the vicinity of the ICB, as illustrated in Fig. 4(c), which reduces the overall stretching and differential advection of the radial background field. Although both Re[$K^{\rm icb}$] and Im[$K^{\rm icb}$] increase in a somewhat monotonic way with $\langle B_r^d\rangle$ (Fig. 5b), the individual contributions from the toroidal and poloidal parts of Im[$K^{\rm icb}$] evolve in a more complex manner (Fig. 5a).

Fig. 6(a) shows how $K^{\rm icb}$ changes as a function of the rms amplitude $\langle B_r\rangle$ of a uniform radial background magnetic field. In this case, $K^{\rm icb}$ is purely toroidal, and once more the result is identical to that of Buffett *et al.* (2002). The case of a uniform radial field is meant to represent the EM coupling when the field morphology includes many different harmonics (e.g. Buffett 1992). Our model allows us to test the uncertainty related to such an approximation. In Figs 6(b) and (c), we show an example of a calculation where the background radial field has a morphology equivalent to that of the antisymmetric (about the equator), non-dipolar part of the

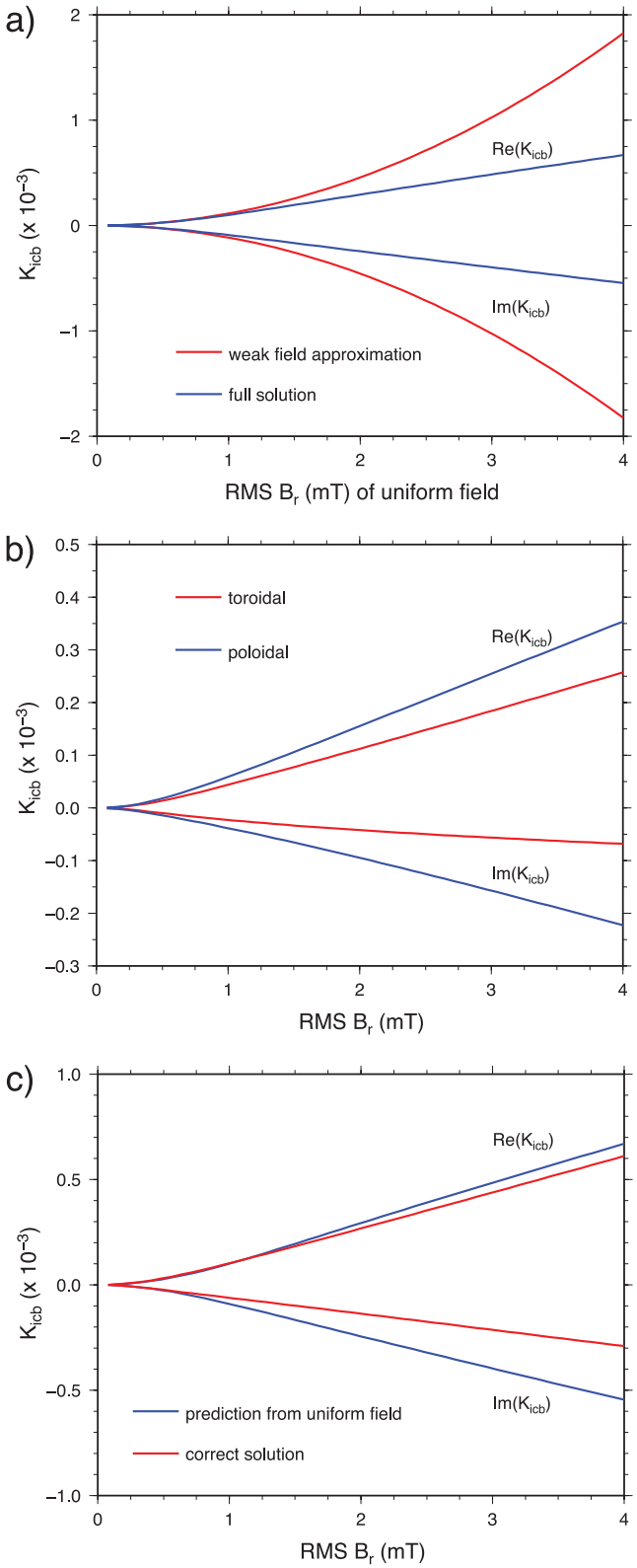

Figure 6. (a) K^{icb} versus rms amplitude of a uniform background field. (b) The toroidal and poloidal contributions, and (c) the total K^{icb} as a function of the rms amplitude of a background radial field model with a morphology equivalent to that of the antisymmetric, non-dipolar part of the field model CHAOS-2s evaluated at the CMB and truncated at degree 5.

field model CHAOS-2s (Olsen *et al.* 2009) evaluated in 2003, at the CMB, and truncated at degree 5. We show both how the partition into the toroidal and poloidal parts of K^{icb} (Fig. 6b) and the total K^{icb} (Fig. 6c) varies as a function of the rms amplitude of this field model. As Fig. 6(c) shows, the magnitude of both Re[K^{icb}] and Im[K^{icb}] is overestimated when an assumed uniform field is used instead of the true field morphology. We have performed calculations similar to that shown in Fig. 6(c) for many different field morphologies. While the exact numerical value of K^{icb} is affected by the field geometry, we find that the magnitude of both Re[K^{icb}] and Im[K^{icb}] are always weaker than if an assumed uniform radial field of equal rms strength is used. The details of these calculations and the reason for this difference will be presented in a forthcoming publication.

5 DISCUSSION AND CONCLUSION

We have shown that the EM coupling model at the ICB and CMB used in nutation studies can be cast under a global formalism, with each variables expanded in spherical harmonics. In the weak field limit, the EM torque is expressed in terms of relatively simple expressions. The evaluation of the torque requires a computation of the coefficients w_{lm}^T and w_{lm}^P which involve the geometry of the background magnetic field. These can be computed by spherical transforms and, provided the truncation degree in spherical harmonic is relatively small (say below 100), such a task is not computationally demanding. Our global model is thus a useful alternative to the model of Buffett *et al.* (2002) based on a 'local' formalism. Moreover, in our model, the poloidal and toroidal parts of the EM torque are evaluated separately, which, as we have illustrated, may be necessary for specific conductivity structures on the solid side of the boundary.

However, in a situation where the strong field regime is appropriate, such as at the ICB, the computational requirements of our global model makes it much less practical to use than a model based on a local formalism. This is not so much a problem in the case of a simple axisymmetric background field, such as an axial dipole or a uniform field; the computation time for these cases is relatively fast. However, for a slightly more complex background magnetic field model, even one containing only low degrees and orders, the eigenvalue problem that must be solved is of a substantial size. This makes the computation quite taxing both on the memory front and execution time. Certainly, schemes can be developed to take advantage of the sparseness of matrices A_f and B to improve the efficiency of the computation, yet this is one more numerical step which is required to obtain solutions. In contrast, in the model based on a local formalism, the computation is straightforward and requires only a single numerical integration over the spherical surface.

Our focus in this study has been on the EM torque in the context of Earth's nutations, but our model can be easily adapted to model the EM torque in other situations. A good example is the axial EM torque on the mantle by decadal timescale flows in the core, resulting in LOD changes. The models developed by Roberts (1972), Stix & Roberts (1984) and Holme (1998) are based on a global formalism, as we have done here, and compute separately the poloidal and toroidal contribution to the torque. Indeed, the model that we have developed here is directly inspired from these. The toroidal part of the torque is evaluated exactly as we have done here, except using a more general core flow in the definition of the forcing (i.e. the toroidal scalar $\mathcal{T}_n$). The poloidal torque, though, was evaluated slightly differently: through a clever manipulation, it is determined directly on the basis of the observed secular variation of the magnetic

field. In certain contexts though, a prediction of the coupling directly in terms of a given core flow, as in our model, is more convenient. An example of this is in the modelling of the normal modes of torsional oscillations (e.g. Braginsky 1970; Buffett 1998; Mound & Buffett 2003; Dumberry & Mound 2008).

ACKNOWLEDGMENTS

M. Dumberry is supported by a NSERC/CRSNG discovery grant (Canada). A part of the work of L. Koot was supported by a post-doctoral fellowship from the National Fund for Scientific Research (FNRS), Belgium.

REFERENCES

Braginsky, S.I., 1970. Torsional magnetohydrodynamic vibrations in the Earth's core and variations in day length, *Geomag. Aeron.,* **10,** 1–10.

Buffett, B.A., 1992. Constraints on magnetic energy and mantle conductivity from the forced nutations of the Earth, *J. geophys. Res.,* **97,** 19 581–19 597.

Buffett, B.A., 1998. Free oscillations in the length of day: inferences on physical properties near the core-mantle boundary, in *The Core-Mantle Boundary Region,* Geophys. Monogr. Vol. 28, pp. 153–165, eds Gurnis, M., Wysession, M.E., Knittle, E. & Buffett, B.A., American Geophysical Union, Washington, DC.

Buffett, B.A., 2010. Tidal dissipation and the strength of the earth's internal magnetic field, *Nature,* **468,** 952–955.

Buffett, B.A., Mathews, P.M. & Herring, T.A., 2002. Modeling of nutation-precession: effects of electromagnetic coupling, *J. geophys. Res.,* **107,** doi:10.1029/2001JB000056.

Christensen, U.R. & Aubert, J., 2006. Scaling properties of convection-driven dynamos in rotating spherical shells and application to planetary magnetic fields, *Geophys. J. Int.,* **166,** 97–114.

Constable, S., 2007. Geomagnetism, in *Treatise on Geophysics,* Vol. 5, chapter 7, pp. 237–276, eds, Schubert, G. & Kono, M., Elsevier, Amsterdam.

Dumberry, M. & Mound, J.E., 2008. Constraints on core-mantle electromagnetic coupling from torsional oscillation normal modes, *J. geophys. Res.,* **113,** B03102, doi:10.1029/2007JB005135.

Edmonds, A.R., 1960. *Angular Momentum in Quantum Mechanics,* Princeton University Press, New Jersey, NJ.

Gillet, N., Jault, D., Canet, E. & Fournier, A., 2010. Fast torsional waves and strong magnetic field within the earth's core, *Nature,* **465,** 74–77.

Greff-Lefftz, M. & Legros, H., 1995. Core mantle coupling and polar motion, *Phys. Earth planet. Inter.,* **91,** 273–283.

Greff-Lefftz, M. & Legros, H., 1999. Magnetic field and rotational eigenfrequencies, *Phys. Earth planet. Inter.,* **112,** 21–41.

Gubbins, D. & Roberts, P.H., 1987. Magnetohydrodynamics of the Earth's core, in *Geomagnetism,* Vol. 2, pp. 1–184, eds Jacobs, J.A., Academic Press, London.

Gwinn, C.R., Herring, T.A. & Shapiro, I.I., 1986. Geodesy by radiointerferometry: studies of the forced nutations of the Earth, 2, interpretation, *J. geophys. Res.,* **91,** 4755–4765.

Hollerbach, R. & Kerswell, R.R., 1995. Oscillatory internal shear layers in rotating and precessing flows, *J. Fluid Mech.,* **298,** 327–339.

Holme, R., 1998. Electromagnetic core-mantle coupling - I. Explaining decadal changes in the length of day, *Geophys. J. Int.,* **132,** 167–180.

Holme, R., 2000. Electromagnetic core-mantle coupling III. Laterally varying mantle conductance, *Phys. Earth planet. Inter.,* **117,** 329–344.

Jackson, A., Jonkers, A. R.T. & Walker, M.R., 2000. Four centuries of geomagnetic secular variation from historical records, *Phil. Trans. R. Soc. Lond., A,* **358,** 957–990.

Mathews, P.M., Herring, T.A. & Buffett, B.A., 2002. Modeling of nutations and precession: new nutation series for nonrigid Earth and insights into the Earth's interior, *J. geophys. Res.,* **107,** doi:10.1029/2004JB000390.

Mound, J.E. & Buffett, B.A., 2003. Interannual oscillations in the length of day: implications for the structure of mantle and core, *J. geophys. Res.,* **108**(B7), 2334, doi:10.1029/2002JB002054.

Munk, W.H. & MacDonald, G.J.F., 1960. *The Rotation of The Earth,* Cambridge University Press, Cambridge.

Olsen, N., Hulot, G. & Sabaka, T.J., 2007. The present field, in *Treatise on geophysics,* Vol. 5, chapter 2, pp. 33–75, eds Schubert, G. & Kono, M., Elsevier, Amsterdam.

Olsen, N., Mandea, M., Sabaka, T.J. & Toffner-Clausen, L., 2009. CHAOS-2 – a geomagnetic field model derived from one decade of continuous satellite data, *Geophys. J. Int.,* **179,** 1477–1487.

Roberts, P.H., 1972. Electromagnetic core-mantle coupling, *J. Geomag. Geoelectr.,* **24,** 231–259.

Rochester, M.G., 1960. Geomagnetic westward drift and irregularities in the Earth's rotation, *Phil. Trans. R. Soc. Lond., A,* **252,** 531–555.

Rochester, M.G., 1962. Geomagnetic core-mantle coupling, *J. geophys. Res.,* **67,** 4833–4836.

Rochester, M.G., 1968. Perturbations in the Earth's rotation and geomagnetic core-mantle coupling, *J. Geomag. Geoelectr.,* **20,** 387–402.

Rochester, M.G., 1976. The secular decrease of obliquity due to dissipative core-mantle coupling, *Geophys. J. R. astr. Soc.,* **46,** 109–126.

Rochester, M.G. & Smylie, D.E., 1965. Geomagnetic core-mantle coupling and the Chandler wobble, *Geophys. J. R. astr. Soc.,* **10,** 289–315.

Sasao, T., 1977. Dissipative core-mantle coupling and nutational motion of the Earth, *Publ. astr. Soc. Japan,* **29,** 83–105.

Stacey, F.D. & Anderson, O.L., 2001. Electrical and thermal conductivities of Fe-Ni-Si alloy under core conditions, *Phys. Earth planet. Inter.,* **124,** 153–162.

Stix, M. & Roberts, P.H., 1984. Time-dependent electromagnetic core-mantle coupling, *Phys. Earth planet. Inter.,* **36,** 49–60.

Toomre, A., 1966. On the coupling of the Earth's core and mantle during the 26 000 yr precession, in *The Earth-Moon system,* pp. 33–45, eds Marsden, B.G. & Cameron, A.G.W., Plenum Press, New York, NY.

Toomre, A., 1974. On the 'nearly diurnal wobble' of the earth, *Geophys. J. R. astr. Soc.,* **338,** 335–348.

Wicht, J. & Jault, D., 2000. Electromagnetic core-mantle coupling for laterally varying mantle conductivity, *J. geophys. Res.,* **105,** 23 569–23 578.